

Mathematical Analysis of ordinary differential equations (ODE)  
and fractional order differential equation (FODE) models of CD70  
CAR T-cell therapy for gliomas

by

**Sujani Ambahera**

A Dissertation

Presented to the Faculty of the Computational Science Program

Middle Tennessee State University

July 2022

---

In Partial Fulfillment

of the Requirements for the Degree

Doctorate of Philosophy in Computational Sciences

---

**Dissertation Committee:**

Dr. Zachariah Sinkala, Chair

Dr. Wandi Ding

Dr. William Robertson

Dr. Qiang Wu

*To my parents*

*Tikiri Banda Ambahera and Kamala Attapattu who have always loved me unconditionally*

*and*

*To my adviser*

*Dr. Zachariah Sinkala, his insights and knowledge in the field of mathematical biology*

*inspired me to explore more in this field*

*and*

*To my husband Sumeda and my children Thiyumi and Yevan*

*who have been a source of strength, patience and support for me throughout this journey.*

# ACKNOWLEDGMENTS

I would like to express my sincere gratitude and appreciation to everyone who has helped me throughout my academic journey. I am extremely grateful to my advisor, Dr. Zachariah Sinkala for his guidance, assistance, encouragement, suggestions, endless patience and countless hours, this research work would not have been possible without him. I am also greatly thankful to the Computational and Data Science Program Director, Dr. John Wallin, for admitting and allowing me to stay in the program and providing me with the financial assistance to complete my graduate studies and research. I am sincerely thankful to my dissertation committee members, Dr. Wandi Ding, Dr. William Robertson and Dr. Qiang Wu for their time, insightful comments, suggestions, and extreme patience. I would like to thank the former chairs, Dr. Donald Nelson, Dr. Lisa Green and chair Dr. Chris Stephens at Department of Mathematical Science for allowing me to teach classes and helping me to gain teaching experience during this program. I want to thank my fellow graduate students in the Computational Science Ph.D. program for their support and assistance. Finally, I am grateful for my parents and my siblings for their support and continuous encouragement. Most importantly, I am grateful to my husband and my children, for their patience, support, and tremendous understanding.

# ABSTRACT

Chimeric antigen receptor T cells (CAR T-cells) immunotherapy has been successful in the treatment of liquid cancers. Currently, CAR T-cells immunotherapy has been investigated for treatment of solid tumors, including glioblastoma (GBM) (brain cancers). Glioma cells with CD70 expression antigen have been identified as a novel potential CAR T target for glioma. Growing evidence from preclinical studies demonstrated that CD70 CAR T-cells can induce potent antitumor response in xenograft and syngeneic models without adverse effects. However, better understanding of the mechanism of CD70 specific CAR T therapy against GBM in immunosuppressive tumor microenvironment requires improving its efficacy. We propose two types of Mathematical models, one is a system of ordinary differential equations (ODEs) and the other is a system of fractional order ordinary differential equations (FODEs) to explore the kinetics of CAR T-cells killing glioma. Although, the ODE model provides very good results with mouse specific CAR T-cells (mCAR T) and human specific CAR T-cells (hCAR T) immunotherapy against glioma in animal models, the cells memory structure becomes significant which the ODE model does take into consideration. The fractional order differential equations model addresses the cell memory structure. The fractional order differential model shows very encouraging results for CAR T immunotherapy against glioma. Computer simulations based on the models using Python and MATLAB programming languages were used to quantify the anti-tumor efficacy of CD70 specific CAR T-cells against gliomas in xenograft and syngeneic mouse models presented in preclinical studies. The models suggests that the success of CAR T-cells treatment depends on individual tumor, tumor growth rate, CD70 level of expression and dose of the treatment.

# TABLE OF CONTENTS

LIST OF TABLES	ix
LIST OF FIGURES	x
<b>CHAPTER 1: INTRODUCTION</b> .....	<b>1</b>
<b>CHAPTER 2: ORDINARY DIFFERENTIAL EQUATION MODEL (ODE MODEL)</b> .....	<b>5</b>
2.1 Published preclinical data . . . . .	5
2.2 Model development (ODE model) . . . . .	6
2.3 Tumor-cell lysis by CAR T-cells . . . . .	7
2.4 ODE model . . . . .	8
2.4.1 Dynamics of Glioma cells ( $G$ ) . . . . .	8
2.4.2 Dynamics of CAR T-cells ( $C_T$ ) . . . . .	9
2.4.3 Dynamics of memory CAR T-cells ( $C_M$ ) . . . . .	10
2.4.4 Dynamics of immune stimulating factor ( $IFN_\gamma$ ) . . . . .	11
2.4.5 Dynamics of immune inhibiting factor ( $TGF_\beta$ ) . . . . .	11
2.4.6 Dynamics of Macrophages ( $M$ ) . . . . .	12
2.5 Proof of theorem of existence of positive solutions and boundness . . . . .	13
2.6 Equilibrium points and Stability analysis . . . . .	17
2.7 Bifurcation analysis . . . . .	18

<b>CHAPTER 3: FRACTIONAL ORDER ORDINARY DIFFERENTIAL EQUATION MODEL (FODE MODEL)</b>	<b>24</b>
3.1 Caputo derivative	25
3.2 Model development (FODE model)	27
3.2.1 Dynamics of Glioma cells ( $G$ )	28
3.2.2 Dynamics of CAR T-cells ( $C_T$ )	29
3.2.3 Dynamics of memory T-cells( $C_M$ )	30
3.2.4 Dynamics of Macrophages ( $M$ )	30
3.2.5 Dynamics of the Cytokine ( $IFN_\gamma$ ).	31
3.2.6 Dynamics of the Cytokine $TGF_\beta$ .	31
3.3 Equilibrium points and Stability analysis	33
3.4 Bifurcation analysis	35
3.4.1 Impact of the fractional order derivative $\theta$ to the stability of the system with small, medium and maximum dosages	38
<b>CHAPTER 4: SENSITIVITY ANALYSIS</b>	<b>41</b>
4.1 Sobol's Sensitivity analysis	41
<b>CHAPTER 5: RESULTS AND ANALYSIS</b>	<b>43</b>
5.1 ODE Model	43
5.1.1 Sensitivity Analysis	44
5.1.2 Parameter Estimation	46
5.1.3 Insights on hCAR T dosing strategy into the elimination of U87 tumor	48
5.1.4 The number of injected hCAR T-cells does affect treatment outcome	48

5.1.5	Maximum expansion of human specific CAR T-cells (hCAR T) at day 7 of injection . . . . .	51
5.1.6	Insights on mCAR T dosing strategy into the elimination of KR70 tumor	52
5.1.7	The number of injected mouse specific CD70 CAR T-cells does affect treatment outcome . . . . .	53
5.1.8	Maximum expansion of mouse specific CAR T-cells (mCAR T) at day 5 of injection . . . . .	54
5.2	FODE Model . . . . .	56
5.2.1	Sobol's sensitivity analysis method . . . . .	56
5.2.2	Model fitting to experimental data . . . . .	59
5.2.3	The impact of inoculation of CAR T-cells on the tumor progression human xenograft glioma model . . . . .	62
5.2.4	The impact of inoculation of non transduced (NT) T or mCAR T-cells on the KR70-C tumor progression in syngeneic glioma models . . . . .	71
5.2.5	The impact of inoculation of non transduced (NT) T or mCAR T-cells on KR70-B tumor progression in syngeneic glioma models . . . . .	74
5.2.6	The comparison of the impact of inoculation of mCAR T-cells on tumor progression in syngeneic glioma models using ODE and FODE models . . . . .	75
5.2.7	The number of injected CAR T-cells does affect treatment outcome . . . . .	77
5.2.8	Maximum expansion of Memory T-cells and CAR T-cells in vivo . . . . .	78
5.3	The effect of memory on the hCAR T-cell therapy against the glioma cells . . . . .	79
5.3.1	The effect of memory on the tumor cells for different values of $\theta$ . . . . .	80

5.3.2	The effect of memory on the hCAR T-cells for different values of $\theta$ . .	82
5.3.3	The effect of memory on the memory T-cells for different values of $\theta$ .	83
<b>CHAPTER 6:</b>	<b>DISCUSSION</b> .....	<b>84</b>
BIBLIOGRAPHY	.....	88

## LIST OF TABLES

1	Parameter values . . . . .	21
2	The Model parameters . . . . .	23
3	Initial values of the model . . . . .	32
4	Parameter values for inequality $V_d^\theta = \frac{e_1^\theta k_1^\theta r^\theta}{M^* \alpha_{11}^\theta \gamma^\theta dosage^\theta} < 1$ . . . . .	36
5	Estimated parameters of growth rate ( $r$ ) and carrying capacity ( $K_G$ ) of glioma cells . . . . .	44
6	The parameter estimates of $d$ , $s$ , $l$ and $w$ for hCAR T and control T cells lysis on CD70+U87 glioma cell lines. . . . .	44
7	The parameter estimates of $d$ , $s$ , $l$ and $w$ for mCAR T and vector T-cells lysis on murine glioma lines KR70. . . . .	44
8	Sobol's Method . . . . .	58

## LIST OF FIGURES

1	Bifurcation diagram (ODE model) . . . . .	19
2	Effect of $V_d$ in varying dosage from small to maximum . . . . .	19
3	Plot of $V_d$ with respect to dosages for ordinary differential equation model. .	22
4	Bifurcation diagram (FODE model). . . . .	35
5	Plot of $V_d^\theta$ with respect to dosages for fractional order differential model. . .	37
6	Plots of $V_d$ with respect to dosages for ordinary differential model and $V_d^\theta$ with respect to dosages for fractional order differential model. . . . .	38
7	Impact of $\theta$ on $V_d^\theta$ with respect to dosages for fractional order differential model.	39
8	The zoom in graph of showing results of impact of $\theta$ on $V_d^\theta$ with respect to dosages for fractional order differential model closer to the medium dosage. .	39
9	Sensitivity analysis in the absence of the data (ODE model) . . . . .	45
10	Sensitivity analysis using data (ODE model) . . . . .	46
11	Dynamics of Glioma cells with hCAR T-cells treatment (ODE model) . . . .	50
12	Dynamics of Memory T-cells with hCAR T-cells treatment(ODE model) . .	51
13	Dynamics of hCAR T-cells (ODE model) . . . . .	52
14	Dynamics of Glioma cells with mCAR T-cells treatment (ODE model) . . .	54
15	Dynamics of mCAR T-cells (ODE model) . . . . .	55
16	Dynamics of Memory T-cells with mCAR T-cells treatment (ODE model) . .	55
17	Sensitivity analysis (FODE model) . . . . .	57

18	Model fit to CAR T-cells data (FODE model) . . . . .	61
19	Glioma cells dynamics with hCAR T-cells treatment for FODE model . . . .	63
20	Dynamics of hCAR T-cells with small, medium and maximum doses treatment of hCAR T-cells (FODE model) . . . . .	63
21	Dynamics of memory T-cells with small, medium and maximum doses of treat- ment of hCAR T-cells (FODE model) . . . . .	64
22	Dynamics of immune stimulating factor with maximum dose of treatment of hCAR T-cells (FODE model) . . . . .	64
23	Dynamics of immune inhibitor factor with small, medium, and maximum doses treatment of hCAR T-cells (FODE model) . . . . .	65
24	Dynamics of microphages with maximum dose ( $10^7$ cells) of treatment of hCAR T-cells (FODE model) . . . . .	65
25	Dynamics of glioma with small, medium and maximum doses of NT T-cells treatment (FODE model) . . . . .	66
26	Dynamics of Glioma, hCAR T and memory T-cells compartments with max- imum treatment observed for first 100 days for FODE model. . . . .	67
27	Dynamics of Glioma, hCAR T and memory T-cells compartments with medium treatment observed for first 100 days for FODE model . . . . .	68
28	Dynamics of Glioma, hCAR T and memory T-cells compartments with small treatment observed for first 100 days for FODE model. . . . .	69
29	Comparison of Glioma cells dynamics for ODE model and FODE model. . .	70
30	hCAR T-cells dynamics for ODE model and FODE model. . . . .	70
31	Memory CAR T-cells dynamics for ODE model and FODE model. . . . .	71

32	Dynamics of glioma cells with mCAR T-cells treatment after 5 days of tumor inoculation (FODE model). . . . .	72
33	Dynamics of glioma cells with mCAR T-cells treatment on day 7 tumor implantation (FODE model) . . . . .	73
34	Dynamics of glioma cells with mCAR T-cells treatment on day 8 tumor implantation (FODE model) . . . . .	74
35	Dynamics of glioma cells with mCAR T-cells treatment on day 18 tumor implantation (FODE model) . . . . .	75
36	The impact of inoculation of mCAR T-cells on tumor progression in syngeneic glioma models using ODE and FODE models. . . . .	76
37	Dynamics of mCAR T-cells (FODE model) . . . . .	77
38	Dynamics Memory CAR T-cells with mCAR T-cells treatment(FODE model)	78
39	The order of the $(\theta)$ impact the dynamics of tumor cells for maximum dosage of hCAR T-cell therapy . . . . .	80
40	The order of the $(\theta)$ impact the dynamics of tumor cells for small dosage of hCAR T-cell therapy . . . . .	81
41	The order of the $(\theta)$ of hCAR T-cells impact the dynamics of hCAR T-cells .	82
42	The order of the $(\theta)$ of memory T-cells impact the dynamics of memory T-cells	83

## CHAPTER 1

### INTRODUCTION

Chimeric antigen receptor T cells (CAR-T cells) therapy is a novel cell-based immunotherapy, in which T cells are genetically engineered to produce receptors on their surface to identify tumor specific antigens. CAR-T cell therapy has shown promising results in liquid cancers (hematologic), but success of CAR T cell therapy in treating solid tumors such as glioblastoma (GBM), a highly aggressive form of primary brain cancer has been limited. CAR T therapy in solid tumors is encountered by numerous challenges, including fewer ideal tumor targets, immunosuppressive tumor microenvironment (TME), tumor heterogeneity, and minimal migration and persistence of CAR T-cells within the tumors. Growing evidence from new studies suggests that antigen CD70, a member of tumor necrosis factor (TNF) receptor super-family, has been emerging as a novel target of CAR T-cell therapy for gliomas. In the study, Ge *et al* [19] found that CD70 expression only on glioma cells and not on normal brain tissue in primary and recurrent GBMs. Jin *et al* [22] reported that CD70 expression is linked with poor survival of malignant gliomas and which may associate with its direct involvement in glioma chemokine productions and selective induction of CD8+ T-cells death. They further demonstrated that targeting CD70-positive tumors with CAR T-cells induces a potent antitumor response in xenograft and syngeneic models without adverse effects. Therefore, their data supported that CD70 is a good target for analyzing CAR-T cell therapy against gliomas. Thus, constructing a mathematical model of CD70 targeted CAR-T cells against tumor cells and its tumor microenvironment (TME) provide better analytical framework for understanding, quantifying and predicting dynamics of CD70 CAR T-cells

killing glioma. In this work, we attempted to investigate the CD70-specific CAR T-cells generate potent anti-tumor response against CD70+ gliomas in xenograft, and syngeneic animal models using system of ordinary differential equations (ODE) and fractional order ordinary differential equation (FODE) models. The mathematical models (ODE and FODE) focus on interaction between glioma cells, CD70 CAR T-cells, memory-T cells, macrophages,  $TGF_{\beta}$  (immune inhibiting factor), and  $IFN_{\gamma}$  (immune stimulating factor) . The mathematical models developed here are built based on the data presented in [22,23] and the structure of the mathematical models presented here are built based on the model presented in [3,39]. The proposed fractional order ordinary differential mathematical model is studied in terms of Caputo fractional derivative due to its properties of non-locality and history or memory containing information. The integer-order derivative is a local operator; hence it is unsuitable in the situation where the problems involve memory and hereditary complex natural phenomena. On the contrary, a fractional derivative has an integral representation which is global phenomena, so it manages to consider these memory and hereditary effects. Fractional calculus is a powerful tool to describe the memory and hereditary properties of the complex natural phenomena. The well-known Riemann-Liouville [51], Grunwald-Letnikov and Caputo operators [6] have been successfully used to model the anomalous structures in many real-world applications. Note that the characteristic property of differential equations (classical and fractional) is the need of specified initial or boundary conditions to guarantee the uniqueness of the solutions. In this sense, Caputo fractional derivative is more preferred than the Riemann-Liouville because it leads to physically interpretable initial conditions. Adam-Bashforth-Moulton (ABM) type predictor-corrector scheme [14] is one of the basic methods for solving fractional derivatives and it has an important place in the Caputo

derivative because the initial conditions are required. For this purpose, we apply the ABM algorithm and illustrate the results by graphics and give stability analysis of treatment free and fixed points of the model.

We perform Sobol's sensitivity analysis to identify the critical parameters that drive the model output linking to glioma cells dynamics. We estimate the model parameters and validate our model using data provided by [2, 3], in which human and mouse CD70-specific CAR T-cells are tested respectively against human primary GBMs and murine glioma lines. The dynamics of the models and some model parameters values are estimated from the data presented in the publications [22], [23]. Simulations of the model also captures the dynamics of other immune system components of our model such as Memory T-cells, macrophages,  $IFN_\gamma$  and  $TGF_\beta$  with various CAR T-cells dosages. We simulated the model with three different CAR T-cells dosages, small, medium and maximum against glioma lines considering two scenarios, one with three different human CD70 CAR T dosages against U87 glioma lines and another with the three different murine-derived CD70 CAR T dosages against KR70 glioma lines using data presented based on a published article from literature [22]. For both cases, our simulated results show that small dosages of CD70 CAR T-cells is not able to eliminate the tumor burden. However, medium and large dosage of CAR T-cells dosage inhibits the tumor burden completely. These simulation results obtained using ODE and FODE models inline with the results which Jin *et al* [22] obtained in their preclinical studies. Bifurcation analysis shows that models exhibit bi-stability where the CAR T-cells threshold dosage exists. If the dosage is above or below the threshold drives the dynamics of glioma in two states. Complete regression or lethal.

This work is assembled as follows: In Chapter 2, we describe the ODE model development

and its biological significance and the quantitative analysis of ODE model involving positivity, boundness, equilibrium points and stability analysis. Chapter 3 consists of the derivation of the fractional order differential equation depicting the interaction between glioma cells and engineered immune system CAR T-cells involves Caputo fractional derivative. It will be followed by the stability analysis of the system of fractional differential equations and fitting model to animal data. In Chapter 4, we explore the sensitivity analysis by performing Sobol's sensitivity analysis method to identify the parameters that have the greatest impact on the model output. Chapter 5 deals with the results, analysis and numerical simulations. Finally, We conclude by presenting the detailed discussion of this work and suggesting directions for future research in Chapter 6.

## CHAPTER 2

### ORDINARY DIFFERENTIAL EQUATION MODEL (ODE MODEL)

#### 2.1 Published preclinical data

In [22],  $5 \times 10^4$  U87.Luc cancer cells were inoculated into the brain of NSG-B2m mice (immunodeficient laboratory mice). Seven days after tumor inoculation, various doses ( $10^5, 10^6, 10^7$  cells per mouse of 8 mice per group) of CD70-specific human CAR T-cells (hCAR T-cells) or control T cells (CTRL or NT T cells (Peripheral Blood Mononuclear Cells (PBMCs) from a healthy donor were adoptively transferred into tumor-bearing NSG-B2m mice. The mice were imaged to monitor tumor growth. They demonstrated that results depend on type of T cells and T cells dose. They reported that complete tumor regressions were observed in KR70-C tumor-bearing mice 17 days after tumor implantation. Significantly prolonged survival was observed in the CAR T treated group of KR70-B tumor-bearing mice compared with the NT T cells treated group, and 38% of the mice were cured by CAR T-cells.

In [22], due to the heterogeneous nature of gliomas, two types of models were used in the study, groups of 6–8 weeks C57BL/6J (the most widely used inbred strain of laboratory mice) mice (10 per group) were inoculated with  $1 \times 10^5$  KR70 tumor cells derived from

- (i) A single clone of a CD70+ glioma cell line, KR70-C,
- (ii) Nonselective bulk CD70-expressing tumors, KR70-B, which expressed various levels of CD70 ( 70% positivity for CD70).

Then ( $1 \times 10^7$ ) NT or mCAR T-cells were adoptively transferred on days 5 and 7 post tumor implantation. They observed complete tumor regressions in KR70-C tumor-bearing mice 17

days after tumor implantation and significantly prolonged survival in the CAR T treated group of KR70-B tumor-bearing mice compared with the NT T cell treated group.

## 2.2 Model development (ODE model)

In this chapter, we propose a six-compartment mathematical model using ordinary differential equations, in which we investigate the interactions between populations of glioma with CD70 expression, effector CAR T-cells (which we just call them CAR T-cells), memory CAR T-cells, macrophages,  $IFN_\gamma$  (immune stimulating factor) and  $TGF_\beta$  (immune inhibiting factor). The mathematical model focuses on CD70 specific CAR T-cell therapy against glioma cells with the aim to simulate and evaluate different therapeutic scenarios. We use mouse CAR T-cells data in animal models from the experiment studies by Jin *et al.* [22] to calibrate and validate our proposed models.

Either population of CD70 CAR T from mice or human is denoted by  $C_T$ . The population of memory CAR T-cells is denoted by  $C_M$  and the population of glioma cells is denoted by  $G$ . The population of macrophages is denoted by  $M$ . Concentration of immune stimulating factor ( $IFN_\gamma$ ) and concentration of immune inhibiting factor ( $TGF_\beta$ ) are denoted by  $I_\gamma$  and  $T_\beta$  respectively.

In order to make useful suggestions about potential treatment plans, we require our model to meet reasonable biological assumptions. We make the following biological assumptions:

1. The Glioma cells growth is logistic without an immune response.
2. Upon contact, CAR T-cells kill glioma cells. In [22], data support that tumor recognition of gliomas by human and mouse CD70 CAR T-cells by  $IFN_\gamma$  release and cytotoxic

killing. They found out that irradiation enhances tumor CD70 expression and CAR T-cells recognition. In our model, we introduce a parameter which scales this recognition of tumor cells by CAR T-cells.

3. CAR T-cells will eventually become inactivated after some number of encounters with glioma cells. CAR T-cells may be stimulated to proliferate upon contact with glioma cells [2, 28]. In [32, 40], it is shown that CAR T-cells are not detected on blood examination after tumor elimination.
4. Memory CAR T-cells are converted to CAR T-cells after contact with tumor cells.
5. CAR T-cells are converted into memory T-cells at a certain constant rate upon reduction of glioma cells.
6. CAR T-cells are inhibited by glioma cells.
7. Memory T-cells have a death rate much smaller than that of CAR T-cells.

Next, we model how CAR T-cells hunt and kill glioma cells.

### 2.3 Tumor-cell lysis by CAR T-cells

The nonlinear fractional kill rate of glioma cells ( $G$ ) by CAR T ( $C_T$ ) cells which is based on the fractional killing of tumor by  $CD8^+$  T cells introduced by De Philis *et al* [11] is given by

$$D(C_T, G)G = \left( \frac{d \left(\frac{C_T}{G}\right)^l}{s + \left(\frac{C_T}{G}\right)^l} \right) G. \quad (1)$$

Where, parameter  $d$  represents saturation level of fractional glioma cells killing by CAR T-cells, and parameter  $s$  represents the steepness coefficient of the glioma- CAR T-cells

competition term.

The above equation is equivalent to the equation below

$$D(C_T, G)G = \frac{dC_T^l G}{sG^l + C_T^l}. \quad (2)$$

When  $l = 1$ ,  $D(C_T, G)G$  becomes the ratio dependent functional response, which is often used in predator-prey models [49]. In this work, we used a more general functional form, Beddington- DeAngelis functional response [4, 9] which cooperates search time. The search time parameter is the time it takes for CAR T-cells to kill glioma cells. Generalized Beddington-DeAngelis functional response of  $C_T$  killing of glioma cells is given by,

$$D(w, C_T, G) = \frac{dC_T^l}{(w + sG^l + C_T^l)}, \quad (3)$$

where  $w$  is related to the search time. When the search time is negligible ( $w = 0$ ), Beddington-DeAngelis functional response becomes ratio dependent functional response.

## 2.4 ODE model

### 2.4.1 Dynamics of Glioma cells ( $G$ )

Next, we model the dynamics of glioma cells with CAR T-cells treatment and the role of macrophages play in killing glioma cells. Combining all the assumptions from above, the dynamics of glioma cells is given by

$$\frac{dG}{dt} = rG \left(1 - \frac{G}{K_G}\right) - \left(\frac{1}{e_1/(\gamma \text{ dosage}) + T_\beta}\right) D(w, C_T, G)G - \left(\frac{\alpha_{11}}{e_1/(\gamma \text{ dosage}) + T_\beta}\right) \left(\frac{G}{G + k_1}\right) M, \quad (4)$$

where,

$$D(w, C_T, G) = \frac{dC_T^l}{(w + sG^l + C_T^l)}.$$

We assume logistic growth pattern for glioma cells with intrinsic growth rate of  $r$  and carrying capacity of  $K_G$ . The logistic growth given by the first term of the Equation (4). The second term of the Equation (4) represents the  $C_T$  induced glioma cells death. The parameter  $\gamma$  scales the CD70 expression of glioma cells. Small value of  $\gamma$  implies that glioma cells have less CD70 expression. The expression  $1/(e_1/\gamma \textit{dosage} + T_\beta)$  of Equation (4) represents the immunosuppressive factor for the activity of CAR T-cells,  $e_1$  being the Michaelis constant.  $D(w, C_T, G)$  is the generalized Beddington–DeAngelis functional response of  $C_T$  killing of glioma cells. Third term of the Equation (4) represents the killing of glioma cells by macrophages with rate of  $\alpha_{11}$  and half saturation constant of  $k_1$ .  $1/(e_1/\gamma \textit{dosage} + T_\beta)$  represents the immunosuppressive factor for the activity of macrophages.

#### 2.4.2 Dynamics of CAR T-cells ( $C_T$ )

We model dynamics of CAR T-cells as follows:

$$\frac{dC_T}{dt} = \alpha_D \left( \frac{D(w, C_T, G)^2 G^2}{K + D(w, C_T, G)^2 G^2} \right) C_T - \alpha_M C_T + \theta_M G C_M - \alpha G C_T - \mu_T C_T. \quad (5)$$

First term of the Equation (5) represents the recruitment of the CD70 specific CAR T-cells by tumor cells. This is a modified Michaelis-Menten term, commonly used in tumor models to govern cells-cells interactions [10, 26, 27]. The degree of the recruitment term is 2, this is the simplest form of the equation best fitting the data provided in [13]. This assumption may not fit our data, hence contributes to the weakness of our model. CAR T-cells differentiate

at the rate  $\alpha_M$  into memory T-cells, which are assumed to provide long lasting protection to the specific glioma/CD70antigen. This means in any future time in which memory T-cells come into contact with tumor cells CD70 expression, memory T-cells are rapidly converted into CD70 CAR T-cells, readily activated to prevent tumor progression, such mechanism is modeled by the term  $\theta_M GC_M$ . Finally, we want our model to reflect the exhaustion or limited activation of CAR T-cells resulting from interaction with a cancer cell [46]. A smaller value of the parameter  $\alpha$  indicates exhaustion or limited activation of CAR T-cells resulting from interaction with cancer cells. The large values of  $\alpha$  represents on average exhaustion and hypo-activation of CAR T-cells, It is not modeled individually. The last term of the Equation (5) shows degradation of CAR T-cells with rate of  $\mu_T$ .

### 2.4.3 Dynamics of memory CAR T-cells ( $C_M$ )

The memory CAR T-cells are modelled by the following equation

$$\frac{dC_M}{dt} = \epsilon\alpha_M C_T - \theta_M GC_M - \mu_M C_M. \quad (6)$$

Memory T-cells  $C_M$  form the immunological memory, a key dynamic of the adaptive immune system [8,45]. The first term of the Equation (6) represents differentiation of CAR T-cells at a rate of  $\epsilon\alpha_M$  to memory T-cells where  $\alpha_M$  is rate of differentiation of  $C_T$  in to  $C_M$ . Since different  $C_T$  cells have different rate of differentiation in to  $C_M$  which is represented by  $\epsilon$ . Parameter  $\epsilon$  is a scalar, value between 0 and 1. As mentioned, when in future contact with the same antigen bearing cancer cells, they immediately return to the effector phenotype at a per capita rate proportional to the tumor burden. In general, memory CAR

T-cells have longevity, and therefore have a much lower mortality rate than the CAR T-cells, i.e.,  $\mu_M \ll \mu_T$  [39]. The dynamics are represented by the Equation (6).

#### 2.4.4 Dynamics of immune stimulating factor ( $IFN_\gamma$ )

The dynamics of  $IFN_\gamma$  denoted by  $I_\gamma$  is modelled by the following equation

$$\frac{dI_\gamma}{dt} = \alpha_0 + \alpha_1 \left( \frac{C_T}{C_T + K_F} \right) - \mu_F I_\gamma. \quad (7)$$

where,  $\alpha_0$  represents the source of interferon gamma. Second term of the Equation (7) gives the production of  $I_\gamma$  by  $C_T$  cells with production rate of  $\alpha_1$  and half saturation constant of  $K_F$ . The third term of the Equation (7) shows the degradation of  $I_\gamma$  with rate of  $\mu_F$ .

#### 2.4.5 Dynamics of immune inhibiting factor ( $TGF_\beta$ )

Next, we develop the Dynamics of immune inhibiting factor ( $TGF_\beta$ ). Evidence from previous studies indicates, the glioma cells themselves secrete immunosuppressive factors such as  $TGF_\beta$ , denoted by  $T_\beta$  [16]. Growth factor  $TGF_\beta$  produced by glioma inhibiting anti-tumor immune surveillance and contributes to glioma progression.

We modelled the dynamics of  $TGF_\beta$  denoted by  $T_\beta$  using the Equation (8)

$$\frac{dT_\beta}{dt} = b_1 G - \mu_2 T_\beta. \quad (8)$$

The first term of the Equation (8) is the source term which is proportional to the glioma size and  $b_1$  being the release rate per glioma cells. The last term is the degradation of  $T_\beta$  at

a constant rate  $\mu_2$ .

#### 2.4.6 Dynamics of Macrophages ( $M$ )

The dynamics of macrophages is governed by the following equation

$$\frac{dM}{dt} = r_M M \left(1 - \frac{M}{K_M}\right) + a_1 \left(\frac{I_\gamma}{k_4 + I_\gamma}\right) \left(\frac{1}{e_2 + T_\beta}\right) - \alpha_3 \left(\frac{G}{G + k_2}\right) M. \quad (9)$$

The first term of the Equation (9) characterizes the logistic growth of the macrophages with intrinsic growth rate of  $r_M$  and carrying capacity of  $K_M$  in the absence of the glioma cells.  $I_\gamma$  is the main cytokine associated with the activation of macrophages. In the second term of the Equation (9), Michaelis–Menten form is used to describe the activation of microphages by  $I_\gamma$  with the activation rate of  $a_1$  and half saturation constant of  $k_4$ . The expression  $\left(\frac{1}{e_2 + T_\beta}\right)$  term represent the interruption of activity of microphages by  $T_\beta$ . The last term of the Equation (9) shows the death of microphages by glioma cells with rate of  $\alpha_3$  and half saturation constant of  $k_2$ .

Thus, each mechanism is modeled individually, which results in the following system of ordinary differential equations:

$$\left\{ \begin{array}{l}
\frac{dG}{dt} = rG \left( 1 - \frac{G}{K_G} \right) - \left( \frac{1}{e_1/(\gamma \text{ dosage}) + T_\beta} \right) D(w, C_T, G)G - \left( \frac{\alpha_{11}}{e_1/(\gamma \text{ dosage}) + T_\beta} \right) \left( \frac{G}{G + k_1} \right) M, \\
\frac{dC_T}{dt} = \alpha_D \left( \frac{D(C_T, G)^2 G^2}{K + D(C_T, G)^2 G^2} \right) C_T - \alpha_M C_T + \theta_M G C_M - \alpha G C_T - \mu_T C_T, \\
\frac{dC_M}{dt} = \epsilon \alpha_M C_T - \theta_M G C_M - \mu_M C_M, \\
\frac{dI_\gamma}{dt} = \alpha_0 + \alpha_1 \left( \frac{C_T}{C_T + K_F} \right) - \mu_F I_\gamma, \\
\frac{dT_\beta}{dt} = b_1 G - \mu_2 T_\beta, \\
\frac{dM}{dt} = r_M M \left( 1 - \frac{M}{K_M} \right) + a_1 \left( \frac{I_\gamma}{K_4 + I_\gamma} \right) \left( \frac{1}{e_2 + T_\beta} \right) - \alpha_3 \left( \frac{G}{G + k_2} \right) M.
\end{array} \right. \tag{10}$$

## 2.5 Proof of theorem of existence of positive solutions and boundness

In this section, we prove existence of positive solutions and boundness of solutions.

### Existence

Since the rates are Lipschitz in terms of the state variables, uniqueness and existence follows easily from [25].

### Positivity

Next, we prove positivity of the solution. From Equation 4, we get

$$\frac{dG(t)}{dt} \geq r_1 G(t) \left( 1 - \frac{G(t)}{G_{max}} \right).$$

Then,

$$G(t) \geq A_1 e^{\int r_1 G(t) \left(1 - \frac{G(t)}{G_{max}}\right) dt} > 0, \text{ for all } t > 0,$$

where  $A_1 = G(0)$  is a positive constant.

From Equation 8 we note that,

$$\frac{dT_\beta}{dt} \geq -\mu_2 T_\beta \text{ (since } G(t) > 0, \text{ for all } t > 0), \quad (11)$$

Then,

$$T_\beta \geq A_2 e^{-\mu_2 t} > 0 \text{ for all } t > 0, \quad (12)$$

where  $A_2 = T_\beta(0)$  is a positive constant.

From Equation 5, we note that,

$$\frac{C_T}{dt} \geq -\alpha_M C_T - \mu_T C_T \text{ (since } G(t) > 0. \text{ for all } t > 0), \quad (13)$$

Then,

$$C_T \geq A_3 e^{-(\alpha_M + \mu_2)t} > 0 \text{ for all } t > 0, \quad (14)$$

where  $A_3 = C_T(0)$  is a positive constant.

From Equation 6

$$\frac{dC_M}{dt} \geq -\mu_M C_M \text{ (since } G(t) > 0, \text{ for all } t > 0), \quad (15)$$

Then,

$$C_M \geq A_4 e^{-\mu_M t} > 0 \text{ for all } t > 0, \quad (16)$$

where  $A_4 = C_M(0)$  is a positive constant.

From Equation 7, we use the following inequality,

$$\frac{dI_\gamma}{dt} \geq -\mu_F I_\gamma \text{ since } \alpha_0 > 0. \quad (17)$$

We deduce that,

$$I_\gamma \geq A_5 e^{-\mu_F t} > 0 \text{ for all } t > 0 \quad (18)$$

where  $A_5 = I_\gamma(0)$  is a positive constant.

From the last Equation 9, we see that,

$$\frac{dM}{dt} \geq r_M M \left( 1 - \frac{M}{K_M} \right) \text{ (since } G(t) > 0, F(t) > 0 \text{ and } T_\beta(t) > 0 \text{ for all } t > 0),$$

Then,

$$M(t) \geq A_6 e^{\int r_M M(t) \left( 1 - \frac{M(t)}{M_{max}} \right) dt} > 0, \text{ for all } t > 0,$$

where  $A_6$  is a positive constant.

## Boundness of solutions

Now, we show the boundness of solutions of the positive solutions in Equation 10. we get the following inequalities. From the equation of the dynamics of glioma cells (Equation 4),

$$\frac{dG(t)}{dt} \leq rG(t) \left( 1 - \frac{G(t)}{G_{max}} \right), \quad (19)$$

Then,

$$G(t) \leq \frac{B_1 G_{max}}{B_1 + e^{r_1 t}}, \quad (20)$$

$$\limsup_{t \rightarrow \infty} G(t) \leq G_{max} = \bar{G}, \quad (21)$$

where  $B_1$  is an arbitrary constant. By using standard Kamke comparison theory [24], from the equation governing  $T_\beta$  (Equation 8)

$$\frac{dT_\beta}{dt} + \mu_2 T_\beta \leq b_1 \bar{G}. \quad (22)$$

Then,

$$T_\beta(t) \leq \frac{b_1 \bar{G}}{\mu_2} (1 - e^{-\mu_2 t}) + B_2 e^{-\mu_2 t}. \quad (23)$$

Hence

$$\limsup_{t \rightarrow \infty} T_\beta(t) \leq \frac{b_1 \bar{G}}{\mu_2} = \bar{T}_\beta(t). \quad (24)$$

From equation governing CAR T-cells (Equation 5), we get

$$\frac{dC_T}{dt} \leq \alpha_D \bar{G} - \rho C_T - \mu_T C_T. \quad (25)$$

$$(26)$$

Then

$$C_T \leq \frac{\alpha_D \bar{G}}{\rho + \mu_T} (1 - e^{-\mu_T t}) + B_3 e^{-\mu_T t}. \quad (27)$$

Hence

$$\limsup_{t \rightarrow \infty} C_T(t) \leq \frac{\alpha_D \bar{G}}{\rho + \mu_T} = \bar{C}_T. \quad (28)$$

From equation 7, we get,

$$\frac{dI_\gamma}{dt} + \mu_F I_\gamma = \alpha_0 + \alpha_1 \left( \frac{C_T}{C_T + K_F} \right). \quad (29)$$

Then, the following inequality,

$$\frac{dI_\gamma}{dt} + \mu_F I_\gamma \leq \alpha_0 + \alpha_1. \quad (30)$$

$$\int_0^t \frac{d}{dt} e^{\mu_F t} I_\gamma \leq (\alpha_0 + \alpha_1) e^{\mu_F t}, \quad (31)$$

$$e^{\mu_F t} I - I_0 \leq \frac{(\alpha_0 + \alpha_1) e^{\mu_F t}}{\mu_F} - \frac{(\alpha_0 + \alpha_1)}{\mu_F}, \quad (32)$$

$$I - e^{-\mu_F t} I_0 \leq \frac{(\alpha_0 + \alpha_1)}{\mu_F} - \frac{(\alpha_0 + \alpha_1) e^{-\mu_F t}}{\mu_F}, \quad (33)$$

$$I \leq \frac{I_0 e^{-\mu_F t}}{\mu_F} + \frac{(\alpha_0 + \alpha_1)}{\mu_F} - \frac{(\alpha_0 + \alpha_1) e^{-\mu_F t}}{\mu_F}, \quad (34)$$

$$I \leq I_0 + \frac{(\alpha_0 + \alpha_1)}{\mu_F}. \quad (35)$$

## 2.6 Equilibrium points and Stability analysis

To study the behavior of the system, we determine the equilibrium points of the system and analyze their stability. To obtain the equilibrium points of the ODE model (10), we set the derivatives to zero,  $\frac{dG}{dt} = 0$ ,  $\frac{dC_T}{dt} = 0$ ,  $\frac{dC_M}{dt} = 0$ ,  $\frac{dF}{dt} = 0$ ,  $\frac{dT_\beta}{dt} = 0$  and  $\frac{dM}{dt} = 0$ .

So, the Equation (4) has two equilibrium points. Tumor-free equilibrium point  $E_1$  which has the zero population of the tumor cells and non-zero tumor equilibrium point  $E_2$  which has the non-zero population of tumor cells.

The tumor-free equilibrium ( $E_1$ ) for all six state variables is given by

$$E_1 = \left( G^* = 0, C_T^* = 0, C_M^* = 0, F^* = \frac{\alpha_0}{\mu_F}, T_\beta^* = 0, M^* \right), \quad (36)$$

where  $M^* = \frac{-b \pm \sqrt{b^2 + 4ac}}{2a}$ ,  $a = -\frac{r_M}{K_M}$ ,  $b = r_M$  and  $c = \frac{(a_1 \alpha_0 K_M)}{(e_2(k_4 + \frac{\alpha_0}{\mu_F}) \mu_F)}$ .

The stability of  $E_1$  is determined by the eigenvalues Jacobian matrix  $J(E_1)$ :

$$J(E_1) = \begin{bmatrix} J_{11} & 0 & 0 & 0 & 0 & 0 \\ 0 & -\alpha_M - \mu_T & 0 & 0 & 0 & 0 \\ 0 & \alpha_M \epsilon & -\mu_M & 0 & 0 & 0 \\ 0 & \frac{\alpha_1}{K_F} & 0 & -\mu_F & 0 & 0 \\ b_1 & 0 & 0 & 0 & -\mu_2 & 0 \\ 0 & 0 & 0 & \frac{a_1}{e_2 k_4} & 0 & -r_M \left( \frac{M^*}{K_M} - 1 \right) - \frac{M^* r_M}{K_M} \end{bmatrix}.$$

Where  $J_{11} = r - \frac{M^* \alpha_{11}}{(e_1/\gamma \text{ dosage}) k_1}$

By computing the Jacobian matrix  $J(E_1)$  of the system, we obtain the eigenvalues of the Jacobian matrix  $J(E_1)$  about the equilibrium point  $E_1$ :

$$\left[ \frac{e_1 k_1 r - \gamma M^* \alpha_{11} \text{dosage}}{e_1 k_1}, \left( \frac{K_M - 2M^*}{K_M} \right) r_M, -\alpha_M - \mu_T, -\mu_M, -\mu_F, -\mu_2 \right].$$

Using parameters in Table 2, we say that the eigenvalues are negative except for first two eigenvalues,  $\frac{e_1 k_1 r - \gamma M^* \alpha_{11} \text{dosage}}{e_1 k_1}$  and  $\left( \frac{K_M - 2M^*}{K_M} \right) r_M$ .

The stability of the tumor free equilibrium point  $E_1$  depends on the above two eigenvalues.

It is stable if  $e_1 k_1 r - M^* \alpha_{11} \gamma \text{dosage} < 0$  and  $(K_M - 2M^*) r_M < 0$ . Namely, if

$e_1 k_1 r - M^* \alpha_{11} \gamma \text{dosage} < 0$ ,  $E_1$  is stable and  $E_2$  is unstable or

$e_1 k_1 r - M^* \alpha_{11} \gamma \text{dosage} > 0$ ,  $E_1$  is unstable and  $E_2$  is stable.

If  $e_1 k_1 r - M^* \alpha_{11} \gamma \text{dosage} < 0$ , tumor cells are killed by CAR T-cells and macrophages. In this case, tumor-free equilibrium point  $E_1$  and the immune system can effectively fight tumor cells.

If  $e_1 k_1 r - M^* \alpha_{11} \gamma \text{dosage} > 0$ , rate of tumor growth is greater than the rate of killing of tumor by CAR T-cells and macrophages.

Non-zero tumor equilibrium point ( $E_2$ ) is given by,

$$E_2 = (G^{**}, C_T^{**}, C_M^{**}, F^{**}, T_\beta^{**}, M^{**}).$$

In this case, we find the value of the non-zero tumor equilibrium point ( $E_2$ ) numerically instead of the analytical equilibrium solutions.

## 2.7 Bifurcation analysis

Local stability of the solutions depends on whether the eigenvalues of jacobian matrix are negative or have negative real part. System consists of tumor free equilibrium point ( $E_1$ )

and non-zero tumor equilibrium ( $E_2$ ). The bifurcation diagram is given in Figure 1.

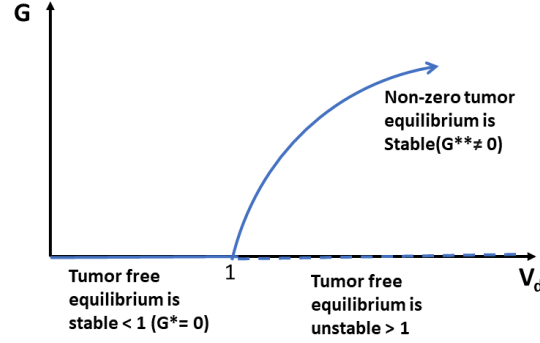


Figure 1: **Bifurcation diagram.** Here,  $G$  represents number of glioma cells and  $V_d = \frac{e_1 k_1 r}{\gamma M^* \alpha_{11} \text{dosage}}$ . Stability of the tumor free equilibrium and the non-zero tumor equilibrium with respect to  $V_d < 1$  and  $V_d > 1$ .

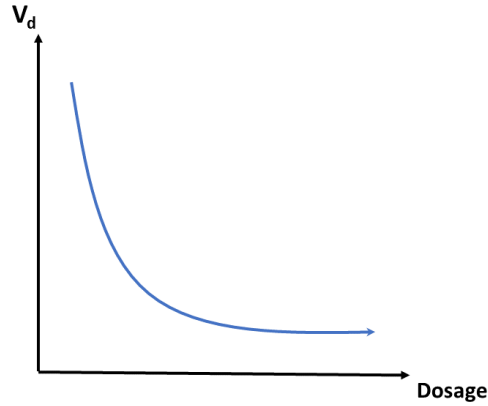


Figure 2: **Effect of  $V_d$  in varying dosage from small to maximum.** Low CAR T dosages have higher  $V_d$  values while maximum dosages have smaller  $V_d$  values.

The eigenvalues of the jacobian matrix  $J(E_1)$  about tumor free equilibrium point  $E_1$  are given by

$$\left[ \frac{e_1 k_1 r - \gamma M^* \alpha_{11} dosage}{e_1 k_1}, \left( \frac{K_M - 2M^*}{K_M} \right) r_M, -\alpha_M - \mu_T, -\mu_M, -\mu_F, -\mu_2 \right].$$

Tumor free equilibrium point  $E_1$  is stable if  $e_1 k_1 r - \gamma M^* \alpha_{11} dosage < 0$  and  $K_M - 2M^* < 0$ .

Tumor free equilibrium point  $E_1$  is unstable otherwise. The above stability condition is equivalent to the following inequality

$$V_d = \frac{e_1 k_1 r}{\gamma M^* \alpha_{11} dosage} < 1. \quad (37)$$

If the tumor free steady state is unstable, the tumor-free equilibrium point and immune system is enough to fight tumor cells. Next, non-zero tumor steady state points are given by  $(G^{**}, C_T^{**}, C_M^{**}, I_\gamma^{**}, T_\beta^{**}, M^{**})$ . For fixed  $M$ , and  $C_T$  and  $T_\beta = \left( \frac{b_1}{\mu_2} \right) G$ , we can show easily that Equation (37) has a unique non-zero positive  $G = G^{**}$

$$r \left( 1 - \frac{G}{K_G} \right) = \frac{D}{(k_1 r) / (\alpha_{11} M^* V_d) + T_\beta} + \frac{\alpha_{11}}{(k_1 r) / (\alpha_{11} M^* V_d) + T_\beta} \frac{M^*}{G + k_1}. \quad (38)$$

Since  $T_\beta = \left( \frac{b_1}{\mu_2} \right) G$  then  $T_\beta^{**}$  is unique if  $G^{**}$  is unique. If  $V_d < 1$  the system has one stable tumor free equilibrium.

Inequality of  $V_d$  in Equation (37) and corresponding Figure 2, show that  $V_d$  decrease with the increase of dosages from small to maximum. Thus, From Figure 1,  $V_d$  drive tumor free equilibrium point to the stability and non-zero tumor equilibrium to unstable state for the smaller values of  $V_d$  ( $V_d < 1$ ).

If  $V_d > 1$  tumor free equilibrium is unstable and non-zero tumor equilibrium is stable.

Similarly, with the increase of dosages from small to maximum, from Figure 1 and Figure 2, we see that,  $V_d$  directs tumor free equilibrium to unstable state and non-zero tumor equilibrium to stability for the values of  $V_d$  greater than 1.

Using Inequality (37) to see how it affect the stability of the system.

$$V_d = \frac{e_1 k_1 r}{\gamma M^* \alpha_{11} \text{dosage}} < 1.$$

Values of the corresponding parameters of the Inequality 37 given by,

Parameter	Value
$e_1$	0.205 $\mu$ gram
$k_1$	$2.7 \times 10^4$ cells
$r$	0.539 $\text{day}^{-1}$
$\alpha_{11}$	$1.5 \times 24 \times 10^{-6}$ $\mu$ gram $\text{day}^{-1}$
$\gamma$	290
$M^*$	$0.98 \times 10^6$ cells

Table 1: Parameter values

We substitute parameter values in Table 1 to Inequality (37) for small ( $0.1 \times 10^6$  cells), medium ( $1.0 \times 10^6$  cells) and maximum ( $10 \times 10^6$  cells) dosages respectively. We found that  $V_d > 1$  for small dosage, see Figure 3. Therefore, system is unstable for small dosage.  $V_d > 1$  for medium and maximum dosages. See Figure 3. Therefore, system is stable for medium and maximum dosages. Biologically, this means small dosage is not able to eliminate the tumor. However, medium and maximum dosages are able to eliminate the tumor. Here, maximum dosage means the largest amount of dosage that one receives with safety.

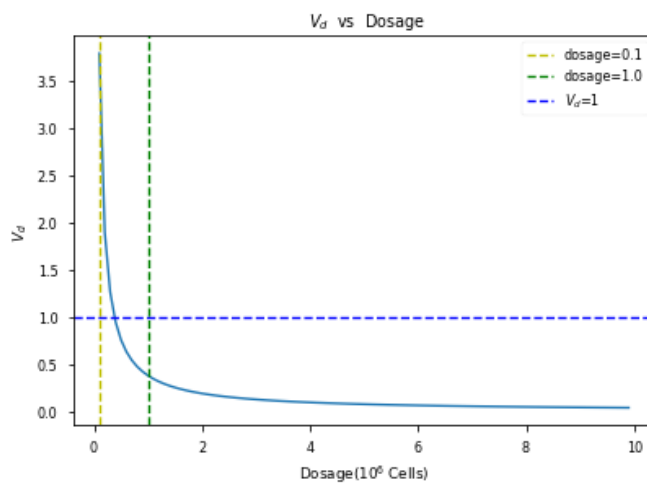


Figure 3: Plot of  $V_d$  with respect to dosages for ordinary differential model.  $V_d > 1$  for small dosage and  $V_d < 1$  for medium and maximum dosages. Therefore, system is unstable for small dosage and stable for medium and maximum dosages.

Parameters	Definitions	values	units	Source
$r$	Growth rate for glioma cells	0.488	/day	Estimated
$K_G$	Carrying capacity of the glioma cells	0.764	$10^6$ cells	Estimated
$e_1$	Michaelis Menten constant	0.01	$\mu$ g	[36]
$\alpha_{11}$	Kill rate of macrophages	0.0036	$\mu$ g/ day	[3]
$k_1$	Half saturation constant	0.027	$10^6$ cells	[31]
$k_5$	Inhibitory parameter	0.02	$\mu$ g	[3]
$\alpha_D$	Maximum $C_T$ cells recruitment rate	0.0375	/day	[13, 27]
$K$	Steepness coefficient of the CAR T-cells recruitment curve	$0.2 \times 10^{-4}$	$10^{12}$ cells <sup>2</sup>	[13, 27]
$\mu_T$	Death rate of $C_T$ cells	$0.1694 \times 24$	/day	[3]
$\theta_M$	Conversion coefficient of $C_M$ into $C_T$ due to interaction with $G$	6	/ $10^6$ cells day	[39]
$\alpha$	Rate of inhibition of glioma cells by $C_T$ cells	0.045	$10^6$ cells day	[39]
$\alpha_M$	Rate of differentiation of $C_T$ in to $C_M$	6	/ $10^6$ cells day	[39]
$\mu_M$	Death rate of macrophages	$0.0194 \times 24$	/ day	[3]
$\alpha_0$	Constant source of $IFN_\gamma$	0.2	/ day	
$\alpha_1$	Rate of activation of $IFN_\gamma$ by $C_T$ cells			
$K_F$	Half-saturation constant	0.095665	$10^6$ cells	
$\mu_F$	Degradation rate of $IFN_\gamma$	$0.102 \times 24$	/ day	[3]
$s_1$	Constant source of $T_\beta$	1.51932	$\mu$ g /day	[3]
$b_1$	Release rate per glioma cell	0.0138	$\mu$ g/ $10^6$ cells day	[3]
$\mu_2$	Degradation of $T_\beta$	$6.93 \times 24$	/ day	[3]
$r_M$	Growth rate for macrophages	$0.330 \times 24$	/ day	[3]
$K_M$	Carrying capacity of the macrophages	1	$10^6$ cells	[3]
$a_1$	Activation rate of macrophages	$2.7912 \times 10^{-6}$	$10^6$ cells	[3]
$K_4$	Half saturation constant	0.0105	$\mu$ g	[44]
$e_2$	Michaelis Menten constant	0.01	$\mu$ g	[36]
$\epsilon$	Scalar	(0 – 1)		[39]

Table 2:

The Model parameters used in the simulation of the system of six differential equations.

## CHAPTER 3

### FRACTIONAL ORDER ORDINARY DIFFERENTIAL EQUATION MODEL (FODE MODEL)

Next, we consider a cancer model using the fractional order ordinary differential equations. Our mathematical model describes the effect of interactions between glioma cells and the immune system, which includes macrophages, CAR T T-cells, memory T-cells,  $TGF\beta$  and  $IFN\gamma$ . As we are dealing with mice lacking immune components, we consider that the CAR T-cells come only from immunotherapy, represented by populations of CAR T lymphocytes (injected into mice). The model focuses on the role of CAR T-cells as immunotherapy to brain tumor, with the aim to simulate and thus evaluate possible therapeutic scenarios and validate the model with experimental results described above in [22]. The mathematical model of the interaction between Glioma cells and engineered immune system CAR T-cells involves Caputo fractional derivative.

Fractional order differential equations have emerged as a powerful mathematical framework to describe dynamical behavior in many fields such as economy, finance, physics, engineering and biology. Non-local property of fractional differential derivative and memory effect of the fractional order differential equations makes mathematical modelling with fractional differential equations more advantages than integer order differential equation models. In particular, fractional differential equations are widely used in biological systems to study dynamical behavior due to the memory effect that is the next state of fractional model depends not only on its current state but also on all of its past states. In this chapter, we study fractional order differential equations to understand the dynamics of CAR T therapy

against glioma cells.

### 3.1 Caputo derivative

There are several approaches to the definition of fractional derivative, Riemann-Liouville, Caputo, and Grünwald-Letnikov etc. In this work, we express fractional derivative in terms of Caputo derivative which is defined below as

$${}^C D_0^\theta y(t) = \frac{1}{\Gamma(m-\theta)} \int_0^t (t-\tau)^{m-\theta-1} y^{(m)}(\tau) d\tau, \quad (39)$$

where,  $\theta$  ( $m-1 < \theta < m, m \in \mathbb{Z}$ ) is the order of the derivative and  $m$  is the smallest integer greater or equal to  $\theta$ ,  $y^{(m-1)}$  is absolutely continuous on  $[0, T]$ . In our case, we consider the case  $m = 1$ . Consider the initial value problem for FODE with Caputo's derivative,

$$D_{t_0}^\theta y(t) = f(t, y(t)) \quad t \in [t_0, T], \quad (40)$$

$$y(0) = y_0, y'(0) = y_0^1, \dots, y^{(m-1)}(0) = y_0^{m-1} \quad (41)$$

where  $f(t, y(t))$  is assumed to be continuous and  $y_0, y_0^{(1)}, \dots, y_0^{(m-1)}$  are the assigned values of the derivatives at  $t_0 = 0$ . Equations (40) and (41) are equivalent to Volterra integral equation [14, 18, 50].

$$y(t) = T_{m-1}[y; 0] + \frac{1}{\Gamma(\theta)} \int_0^t (t-\tau)^{\theta-1} f(\tau, y(\tau)) d\tau, \quad (42)$$

where  $T_{m-1}[y; 0](t)$  is the Taylor polynomial of degree  $m-1$  for the function  $y(t)$  centered at  $t = 0$ , that is:

$$T_{m-1}[y; 0](t) = \sum_{k=0}^{m-1} y^{(k)}(0) \frac{t^k}{k!}. \quad (43)$$

To determine a discrete solution, we first discretize the time domain  $[0, T]$ . Now we use evenly spaced points,  $t_j, j=0, 1, 2, \dots, N-1$  as follow,

$$0 = t_0 < t_1, \dots < t_j < \dots < t_n < t_{n+1} < t_N = T, \text{ where, step size is given by } h = t_{j+1} - t_j.$$

A solution of Equation 42 can be expressed as a set of three terms [30],

$$y(t_{n+1}) = T_{m-1}[y; 0](t_{n+1}) + y^*(t_{n+1}) + Y(t_{n+1}). \quad (44)$$

where  $y^*(t_{n+1})$  is the lag term which describe the memory effect in fractional order differential equations and  $Y(t_{n+1})$  is the increment term. lag term  $y^*(t_{n+1})$  is defined by,

$$y^*(t_{n+1}) = \frac{1}{\Gamma(\theta)} \int_0^{t_n} (t_{n+1} - \tau)^{\theta-1} f(\tau, y(\tau)) d\tau. \quad (45)$$

The increment term  $Y(t_{n+1})$  is described by

$$Y(t_{n+1}) = \frac{1}{\Gamma(\theta)} \int_{t_n}^{t_{n+1}} (t_{n+1} - \tau)^{\theta-1} f(\tau, y(\tau)) d\tau. \quad (46)$$

We can rewrite Equation (44) as below,

$$y(t_{n+1}) = T_{m-1}[y; 0](t_{n+1}) + \frac{1}{\Gamma(\theta)} \int_0^{t_n} (t_{n+1} - \tau)^{\theta-1} f(\tau, y(\tau)) d\tau + \frac{1}{\Gamma(\theta)} \int_0^{t_n} (t_{n+1} - \tau)^{\theta-1} f(\tau, y(\tau)) d\tau. \quad (47)$$

Adams-Bashforth-Moulton approach [14] is used to construct the predictor–corrector method. Predictor–corrector method is applied to the Equation 47 to obtain the numerical solution of the fractional order differential equations (FODE). Predictor–corrector method uses an explicit method for the predictor step and an implicit method for the corrector step.

### 3.2 Model development (FODE model)

We develop a mathematical model for the growth and control of glioma cells by administering various doses of the CD70 CAR T-cells adoptively transferred into the tumor  $t \in \{5, 7, 8, 18\}$  days after tumor inoculation, using a system of six non-linear coupled fractional ordinary differential equations (FODEs), which captures the interactive dynamics of glioma cells (malignant brain tumor), macrophages, CD70 CAR T-cells, memory CAR T-cells, immunosuppressive cytokine ( $TGF\beta$ ) and immuno-stimulatory cytokine ( $IFN\gamma$ ).

The state variables of the mathematical model that describes the temporal changes of the kinetics of six population are as follows: namely, malignant gliomas  $G(t)$ , macrophages  $M(t)$ , CD70 CAR T-cells  $C_T(t)$ , memory CAR T-cells  $C_M(t)$ , immunosuppressive factor ( $TGF\beta(t)$ )  $T_\beta(t)$ , and immuno-stimulatory factor ( $IFN\gamma(t)$ )  $I_\gamma(t)$ .

The glioma cells grow logistically with growth rate and carrying capacity  $r^\theta$  and  $K_G^\theta$  respectively. A term representing the fractional cell kill of tumor cells by CAR T-cells is given by the nonlinear function  $D(\theta, w, C_T, G)$ . The function  $D(\theta, w, C_T, G)$  is the generalization of the Beddington–DeAngelis functional response [4, 9, 49] which considers the search time, handling time, and predator interference. For  $w = 0, \theta = 1$ , the function  $D$  depends on the populations  $C_T$  and  $G$  but the experimental data in [13], show that percent lysis appears to be a function of the ratio of CAR T-cells to tumor cells [10]. In the term  $D(\theta, w, C_T, G)G =$

$$\frac{d C_T^{l^\theta} G}{w^\theta + s^\theta G^{l^\theta} + C_T^{l^\theta}},$$

If  $\theta=1, w=0$ ,  $D(1, 0, C_T, G)$  is the ratio-dependent functional response, which has been used in predator–prey models. The ratio-dependent functional response considers the handling time and the time wasted due to predator interference. This can be interpreted as the

time it takes for CAR T-cells to kill tumor cells and the time wasted due to the encounters between CAR T-cells. When the search time is neglectable, the Beddington–DeAngelis functional response becomes the ratio-dependent functional response. Hence  $D(\theta, 0, C_T, G)G$  assumes that the time it takes for CAR T-cells to seek or recognize tumor cells is neglectable. In this work, the search time is incorporated in tumor cells lysis by CAR T-cells.

Other parameters involved are  $d^\theta$ ,  $s^\theta$  and  $\theta$  representing the saturation level of fractional tumor cells kill by CAR T-cells, steepness coefficient of the tumor lysis term  $D(\theta, w, C_T, G)$ , and order of the fractional derivative, respectively [1].

Note that when the search parameter  $w = 0$  the tumor-free equilibrium in Equations is asymptotically stable [48]. When the search time is positive, the effectiveness of tumour cells lysis decreases. Since in here we are considering two type of CAR T-cells hCAR T, and mCAR T-cells, we denote  $w_h$  and  $w_m$  parameters associated with search time for hCAR T and mCAR T-cells respectively.

### 3.2.1 Dynamics of Glioma cells ( $G$ )

The dynamics of glioma cells is given by

$$\frac{d^\theta G}{dt} = r^\theta G \left( 1 - \frac{G}{K_G^\theta} \right) - \frac{DG}{(e_1/(\gamma \text{ dosage}))^\theta + T_\beta} - \frac{\alpha_{11}^\theta}{(e_1/(\gamma \text{ dosage}))^\theta + T_\beta} \frac{GM}{G + k_1^\theta}. \quad (48)$$

We assume that in the absence of immune system glioma cells follow logistic growth, given by the first term of the Equation (48),  $r^\theta$  is the intrinsic growth rate of glioma cells and  $K_G^\theta$  is its carrying capacity, that is, the maximal tumor burden.  $r^\theta$ ,  $K_G^\theta$  and  $\theta$  are estimated by using the logistic model for tumor growth:

$$\frac{d^\theta G}{dt} = r^\theta G \left( 1 - \frac{G}{K_G^\theta} \right). \quad (49)$$

and using data from in [19], Figure 2. The second and third terms of Equation (48) shows the tumor growth inhibited by CAR T-cells and macrophages. The fractional killing rate by CAR T-cells is represented by  $D$ . The glioma cells are eradicated by the macrophages at the rates  $\alpha_{11}^\theta$ . The factor  $\frac{1}{(e_1/(\gamma \text{ dosage}))^\theta + T_\beta}$  is the major immunosuppressive factor for the activity of both the macrophages and CAR T-cells,  $e_1^\theta$  being the Michaelis constant are proportional to both  $G, C_T$  and  $G, M$  respectively, with saturation for large  $G$ . Michaelis Menten term is being incorporated to bring out the accessibility of the glioma cells to macrophages and CAR T-cells, implying that the effect of macrophages and CAR T-cells efficacy follow Michaelis-Menten saturation dynamics,  $k_1^\theta$  being the half saturation constant.

### 3.2.2 Dynamics of CAR T-cells ( $C_T$ )

CAR T-cells dynamics is given by

$$\frac{d^\theta C_T}{dt} = \frac{\alpha_D^\theta D^2 G^2}{K^\theta + D^2 G^2} C_T - \alpha_M^\theta C_T + \theta_M^\theta G C_M - \alpha^\theta G C_T - \mu_T^\theta C_T. \quad (50)$$

The first term in the Equation (50) represents the recruitment term of CAR T-cells are activated by a number of triggers, including fragments of tumor cells that have been killed by other CAR T-cells [21]. The second term represents CAR T-cells differentiate rate at a rate  $\alpha_M^\theta$  into long-term memory T-cells, which are assumed to provide long lasting protection to the specific tumor/antigen. This means that at any future time in which memory T-cells come into contact with same tumor cells, memory T-cells are able to rapidly be converted into CAR T-cells, readily activated to prevent tumor progression. Such mechanism is modeled by the third term  $\theta_M^\theta G C_M$ . Finally, CAR T-cells may be inhibited due to tumor modulated immunosuppressive mechanisms according to the second last term  $\alpha^\theta G C_T$ . The last term

represents death rate of CAR T-cells.

### 3.2.3 Dynamics of memory T-cells( $C_M$ )

Memory T-cells are activated by tumor cells. This is a simplification of the intricate mechanism by which the tumor antigens activate the memory T-cells. Here we consider only the effects associated with the activation of memory T-cells by the tumor, which provides a rapid response to the presence of the target antigen presented by the tumor [35]. Memory T-cell dynamics is given by

$$\frac{d^\theta C_M}{dt} = (\epsilon\alpha_M)^\theta C_T - \theta_M^\theta G C_M - \mu_M^\theta C_M. \quad (51)$$

The first term represents differentiation of CAR T-cells at a rate  $(\epsilon\alpha_M)^\theta$  to memory CAR T-cells, Since different  $C_T$  cells have different rate of differentiation in to  $C_M$  which is represented by  $\epsilon$ . Parameter  $\epsilon$  is a scalar, value between 0 and 1. Since we are dealing with immunodeficient mice. The second term represents contact with rate of the phenotype change when memory T-cells contact the same antigenbearing cancer cells, they immediately return to the CAR T-cells at a per capita rate proportional to the tumor burden. The last term represents the death rate of memory T-cells at the rate  $\mu_M^\theta$ .

### 3.2.4 Dynamics of Macrophages ( $M$ )

Dynamics of macrophages,  $M$  is described by the Equation (52):

$$\frac{d^\theta M}{dt} = r_M^\theta M \left( 1 - \frac{M}{K_M^\theta} \right) + a_1^\theta \frac{I_\gamma}{k_4^\theta + I_\gamma} \frac{1}{e_2^\theta + T_\beta} - \alpha_3^\theta \frac{G}{G + k_2^\theta} M. \quad (52)$$

The first term represents the macrophages logistic growth in absence of glioma cells with intrinsic growth rate  $r_M^\theta$  and carrying capacity  $K_M^\theta$ . The second term in Equation (52) shows the activation of macrophages by  $I_\gamma$  at a rate  $a_1$ ,  $k_4^\theta$  being the half saturation constant, implying the presence of Michaelis-Menten saturation dynamics. At the same time, the term  $\frac{1}{e_2^\theta + T_\beta}$  interrupts the activity of macrophages, it is a degradation term with saturation constant  $e_2^\theta$ . The third term gives the rate of immuno-induced macrophage death by malignant glioma cells at the rate  $\alpha_3^\theta$ ,  $k_2^\theta$  being the half saturation constant standing for the accessibility of glioma cells to macrophages.

### 3.2.5 Dynamics of the Cytokine ( $IFN_\gamma$ ).

Equation (53) represents the dynamics of  $IFN_\gamma$  denoted by  $I_\gamma$ ,

$$\frac{d^\theta I_\gamma}{dt} = \alpha_0^\theta + \alpha_1^\theta \frac{C_T}{C_T + K_F^\theta} - \mu_F^\theta I_\gamma. \quad (53)$$

Immune stimulating factor  $IFN_\gamma$  activates the macrophages, which are capable of destroying the glioma cells. We assume that CAR T-cells is a source of  $I_\gamma$  given by the first two terms of the Equation (53). The last term shows the degradation of  $I_\gamma$  at a constant rate  $\mu_F^\theta$ .

### 3.2.6 Dynamics of the Cytokine $TGF_\beta$ .

Experimental evidence [12] suggests that  $TGF_\beta$  is produced in a small quantity when production of glioma cells is small, but it gets ample nutrient from the neighboring tissue. But when glioma cells production grows sufficiently large resulting in lack of oxygen and space, it starts producing  $TGF_\beta$  to destroy immune response for tumor growth [34]. Equation (54)

describes the dynamics of  $TGF_\beta$  denoted by  $T_\beta$ :

$$\frac{d^\theta T_\beta}{dt} = b_1^\theta G - \mu_2^\theta T_\beta. \quad (54)$$

The first term in Equation (54) represents the source term which is proportional to the glioma size,  $b_1^\theta$  being the release rate per glioma cells. The last term is the degradation of  $TGF_\beta$  at a constant rate  $\mu_2^\theta$ .

Thus our fractional model is given as follows:

$$\left\{ \begin{array}{l} \frac{d^\theta G}{dt} = r^\theta G \left( 1 - \frac{G}{K_G^\theta} \right) - \frac{DG}{(e_1/(\gamma \text{ dosage}))^\theta + T_\beta} - \frac{\alpha_{11}^\theta}{(e_1/(\gamma \text{ dosage}))^\theta + T_\beta} \frac{GM}{G + k_1^\theta}, \\ \frac{d^\theta C_T}{dt} = \frac{\alpha_D^\theta D^2 G^2}{K^\theta + D^2 G^2} C_T - \alpha_M^\theta C_T + \theta_M^\theta G C_M - \alpha^\theta G C_T - \mu_T^\theta C_T, \\ \frac{d^\theta C_M}{dt} = (\epsilon \alpha_M)^\theta C_T - \theta_M^\theta G C_M - \mu_M^\theta C_M, \\ \frac{d^\theta M}{dt} = r_M^\theta M \left( 1 - \frac{M}{K_M^\theta} \right) + a_1^\theta \frac{I_\gamma}{k_4^\theta + I_\gamma} \frac{1}{e_2^\theta + T_\beta} - \alpha_3^\theta \frac{G}{G + k_2^\theta} M, \\ \frac{d^\theta I_\gamma}{dt} = \alpha_0^\theta + \alpha_1^\theta \frac{C_T}{C_T + K_F^\theta} - \mu_F^\theta I_\gamma, \\ \frac{d^\theta T_\beta}{dt} = b_1^\theta G - \mu_2^\theta T_\beta. \end{array} \right. \quad (55)$$

Variable	Symbol	Value
Glioma cells	$G$	$5 \times 10^4$ cells
CAR T-cells	$C_T$	$10^5 - 10^7$ cells
Memory CAR T-cells	$C_M$	0 cells
Macrophages	$M$	0 cells
Immune inhibiting factor	$T_\beta$	0 grams
Immune stimulating factor	$I_\gamma$	0 grams

Table 3:

In the model, all state variables have initial value zero except glioma cells. The CAR T-cells have zero initial value. Then after  $t \in \{5, 7, 8, 18\}$  days there is an injection of CAR T-cells.

### 3.3 Equilibrium points and Stability analysis

The equilibrium points for fractional derivative model (55) are solutions of Equations (56):

$$\left\{ \begin{array}{l} r^\theta G \left( 1 - \frac{G}{K_G^\theta} \right) - \frac{DG}{(e_1/(\gamma \text{ dosage}))^\theta + T_\beta} - \frac{\alpha_{11}^\theta}{(e_1/(\gamma \text{ dosage}))^\theta + T_\beta} \frac{GM}{G + k_1^\theta} = 0, \\ \frac{\alpha_D^\theta D^2 G^2}{K^\theta + D^2 G^2} C_T - \rho^\theta C_T + \theta_M^\theta G C_M - \alpha^\theta G C_T - \mu_T^\theta C_T = 0, \\ (\epsilon \alpha_M)^\theta C_T - \theta_M^\theta G C_M - \mu_M^\theta C_M = 0, \\ r_M^\theta M \left( 1 - \frac{M}{K_M^\theta} \right) + a_1^\theta \frac{I_\gamma}{k_4^\theta + I_\gamma} \frac{1}{e_2^\theta + T_\beta} - \alpha_3^\theta \frac{G}{G + k_2^\theta} M = 0, \\ \alpha_0^\theta + \alpha_1^\theta \frac{C_T}{C_T + K_F^\theta} - \mu_F^\theta I_\gamma = 0, \\ b_1^\theta G - \mu_2^\theta T_\beta = 0. \end{array} \right. \quad (56)$$

So, the system (56) has two equilibrium points

$$E_1 = \left( G^* = 0, C_T^* = 0, C_M^* = 0, M^*, I_\gamma^* = \frac{\alpha_0^\theta}{\mu_F^\theta}, T_\beta^* = \frac{s_1^\theta}{\mu_2^\theta} \right), \quad (57)$$

where

$$M^* = \frac{b + \sqrt{b^2 + 4ac}}{2a}, \quad a = r_M^\theta, \quad b = (r_M K_M)^\theta, \quad c = \frac{(a_1 \alpha_0 K_M)^\theta}{\left( e_2^\theta (k_4^\theta + \frac{\alpha_0^\theta}{\mu_F^\theta}) \mu_F^\theta \right)}.$$

The second equilibrium point can be shown that it does exist and is unique, we call it,  $E_2$ ,

$$E_2 = (G^{**}, C_T^{**}, C_M^{**}, M^{**}, I_\gamma^{**}, T_\beta^{**}).$$

The stability of equilibrium points  $E_1$  and  $E_2$  can be deduced by the eigenvalues of the system Jacobian matrix  $J(E)$ . The stability of  $E_1$  is determined by the eigenvalues Jacobian matrix  $J(E_1)$ :

$$J(E_1) = \begin{bmatrix} J_{11} & 0 & 0 & 0 & 0 & 0 \\ 0 & -\rho^\theta & 0 & 0 & 0 & 0 \\ 0 & \alpha_M^\theta & -\mu_M^\theta & 0 & 0 & 0 \\ -\frac{M^* \alpha_3^\theta}{k_2^\theta} & 0 & 0 & -r_M^\theta \left(2 \frac{M^*}{K_M^\theta} - 1\right) & \frac{\alpha_1(1-F^*)}{(F+k_4^\theta)e_2^\theta} & -\frac{F a_1}{(F+k_4^\theta)(e_2^\theta)^2} \\ 0 & \frac{\alpha_1^\theta}{K_F^\theta} & 0 & 0 & -\mu_F^\theta & 0 \\ b_1^\theta & 0 & 0 & 0 & 0 & -\mu_2^\theta \end{bmatrix},$$

$$\text{where } J_{11} = r^\theta - \frac{M^* \alpha_{11}^\theta}{k_1^\theta (e_1 / (\gamma \text{ dosage}))^\theta} = \frac{r^\theta k_1^\theta e_1^\theta - M^* \alpha_{11}^\theta (\gamma \text{ dosage})^\theta}{k_1^\theta e_1^\theta}.$$

The local stability of the solution depends on whether the eigenvalues of the jacobian are negative or have negative real part. By computing the Jacobian matrix  $J(E_1)$  of the system, we obtain the eigenvalues of the Jacobian matrix  $J(E_1)$  about the equilibrium point  $E_1$ :

$$\left[ \frac{e_1^\theta k_1^\theta r^\theta - \gamma^\theta M^* \alpha_{11}^\theta \text{ dosage}^\theta}{e_1^\theta k_1^\theta}, \frac{(K_M^\theta - 2 M^*) r_M^\theta}{K_M^\theta}, -\rho^\theta, -\mu_M^\theta, -\mu_F^\theta, -\mu_2^\theta \right].$$

Using by parameters in Table 5, we see that the eigenvalues are negative except for first two eigenvalues,  $\frac{e_1^\theta k_1^\theta r^\theta - \gamma^\theta M^* \alpha_{11}^\theta \text{ dosage}^\theta}{e_1^\theta k_1^\theta}$  and  $\frac{(K_M^\theta - 2 M^*) r_M^\theta}{K_M^\theta}$ .

The stability of the tumor free equilibrium point  $E_1$  depends on the above two eigenvalues.

It is stable if  $e_1^\theta k_1^\theta r^\theta - M^* \alpha_{11}^\theta \gamma^\theta \text{ dosage}^\theta < 0$  and  $(K_M^\theta - 2 M^*) r_M^\theta < 0$ . Namely, if

$e_1^\theta k_1^\theta r^\theta - M^* \alpha_{11}^\theta \gamma^\theta \text{ dosage}^\theta < 0$ ,  $E_1$  is stable and  $E_2$  is unstable or

$e_1^\theta k_1^\theta r^\theta - M^* \alpha_{11}^\theta \gamma^\theta \text{ dosage}^\theta > 0$ ,  $E_1$  is unstable and  $E_2$  is stable.

If  $e_1^\theta k_1^\theta r^\theta - M^* \alpha_{11}^\theta \gamma^\theta \text{ dosage}^\theta < 0$ , tumor cells are killed by CAR T-cells and macrophages.

In this case, tumor-free equilibrium point  $E_1$  and the immune system can effectively fight and kill tumor cells.

if  $e_1^\theta k_1^\theta r^\theta - M^* \alpha_{11}^\theta \gamma^\theta \text{ dosage}^\theta > 0$ , rate of tumor growth is greater than the rate of killing of tumor by CAR T-cells and macrophages.

Bifurcation analysis shows that model exhibits bi-stability where the CAR T-cells threshold dosage exists. If the dosage is above or below the threshold drives the dynamics of glioma in two states. Complete regression or lethal, see Figure 4.

The bifurcation diagram is given in Figure 4.

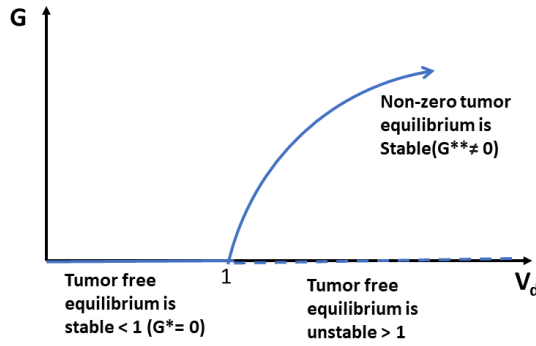


Figure 4: Bifurcation diagram (FODE model). Forward bifurcation diagram with respect to  $V_d$ , where

$$V_d^\theta = \frac{e_1^\theta k_1^\theta r^\theta}{M^* \alpha_{11}^\theta (\gamma \text{ dosage})^\theta} \text{ and } G \text{ is such that } r^\theta \left(1 - \frac{G}{K_G^\theta}\right) = \frac{D}{(k_1 r)^\theta / (\alpha_{11}^\theta M^* V_d) + T_\beta} + \frac{\alpha_{11}^\theta}{(k_1 r)^\theta / (\alpha_{11}^\theta M^* V_d) + T_\beta} \frac{M}{G + k_1^\theta}.$$

$V_d = 1$  is a bifurcation point.

### 3.4 Bifurcation analysis

The above stability condition is equivalent to the following Inequality (58)

$$V_d^\theta = \frac{e_1^\theta k_1^\theta r^\theta}{M^* \alpha_{11}^\theta \gamma^\theta \text{ dosage}^\theta} < 1. \quad (58)$$

If the tumor free steady state is stable, the tumor-free equilibrium point and immune system is enough to fight tumor cells. Next, non-zero tumor steady state points are given by

$(G^{**}, C_T^{**}, C_M^{**}, I_\gamma^{**}, T_\beta^{**}, M^{**})$ . For fixed  $M$ , and  $C_T$  and  $T_\beta = \left(\frac{b_1}{\mu_2}\right)^\theta G$ , we can show easily

that Equation (59) has a unique non-zero positive  $G = G^{**}$

$$r^\theta \left(1 - \frac{G}{K_G^\theta}\right) = \frac{D}{(k_1 r)^\theta / (\alpha_{11}^\theta M^* \mathcal{V}_d) + T_\beta} + \frac{\alpha_{11}^\theta}{(k_1 r)^\theta / (\alpha_{11}^\theta M^* \mathcal{V}_d) + T_\beta} \frac{M}{G + k_1^\theta}. \quad (59)$$

Since  $T_\beta = \left(\frac{b_1}{\mu_2}\right)^\theta G$  then  $T_\beta^{**}$  is unique if  $G^{**}$  is unique.

If  $V_d < 1$  the system has one stable tumor free equilibrium. If  $V_d > 1$  tumor free equilibrium is unstable and non-zero tumor equilibrium is stable. Hence When  $V_d = 1$  we have a bifurcation point, see Figure 4.

From (58),

$$V_d^\theta = \frac{e_1^\theta k_1^\theta r^\theta}{M^* \alpha_{11}^\theta \gamma^\theta \text{dosage}^\theta} < 1.$$

Parameter	Value
$e_1$	0.266 $\mu$ gram
$k_1$	$2.7 \times 10^4$ cells
$r$	0.539 $day^{-1}$
$\alpha_{11}$	$1.5 \times 24 \times 10^{-6}$ $\mu$ gram $day^{-1}$
$\gamma$	290
$\theta$	0.77155
$M^*$	$0.98 \times 10^6$ cells

Table 4: Parameter values for inequality  $V_d^\theta = \frac{e_1^\theta k_1^\theta r^\theta}{M^* \alpha_{11}^\theta \gamma^\theta \text{dosage}^\theta} < 1$ .

We substitute parameter values in Table 4 to Inequality (58) considering three dosages, small ( $0.1 \times 10^6$  cells), medium ( $1.0 \times 10^6$  cells) and maximum ( $10 \times 10^6$  cells) respectively. We plot  $V_d^\theta$  with varying dosages by fixing other parameters in inequality 58 and found that  $V_d^\theta > 1$  for small dosage. See Figure 5, therefore, system is unstable for small dosage,

and it is not able to eliminate the tumor.  $V_d^\theta < 1$  for medium and maximum dosages, see Figure 5, therefore, system is stable for medium and maximum dosages. However, medium and maximum dosages are able to eliminate the tumor completely. Here, maximum dosage means the largest amount of dosage that one receives with safety [22].

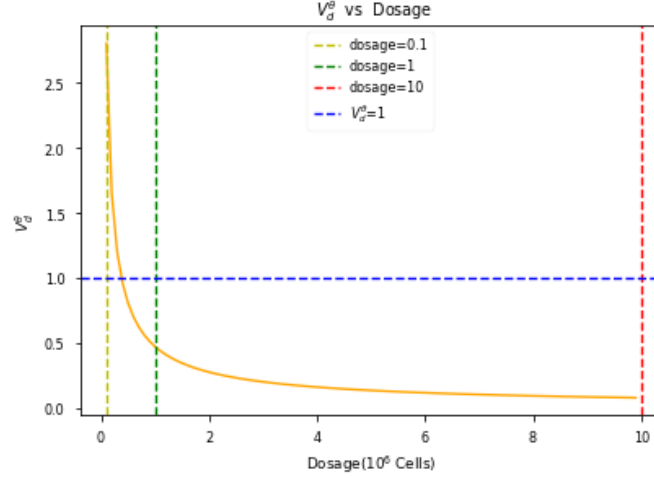


Figure 5: Plot of  $V_d^\theta$  with respect to dosages for fractional order differential model.  $V_d^\theta > 1$  for small dosage and  $V_d^\theta < 1$  for medium and maximum dosages, where  $V_d^\theta = \frac{\epsilon_1^\theta k_1^\theta r^\theta}{M^* \alpha_{11}^\theta (\gamma \text{ dosage})^\theta}$ .

We plotted  $V_d$  with respect to dosages for the ordinary differential equation model and  $V_d^\theta$  with respect to dosages for the fractional differential equation model in the same graph (see Figure 6) to see how the memory affect the stability of the systems. For small dosage,  $V_d$  and  $V_d^\theta$  values are greater than 1 in both models. For medium and maximum dosages,  $V_d$  and  $V_d^\theta$  values are less than 1.

We found that the threshold CAR T dosage is  $0.48 \times 10^6$  cells which is the minimum CAR T dosage that eliminate the cancer. The X-coordinates of the intersection of the orange and blue plots and  $V_d=1$  line in Figure 6 shows the threshold dosage for both models. CAR T dosage below this threshold dosage is not able to eliminate the tumor and cancer will grows

to its lethal size. CAR T dosage above this threshold dosage is able to eliminate the cancer.

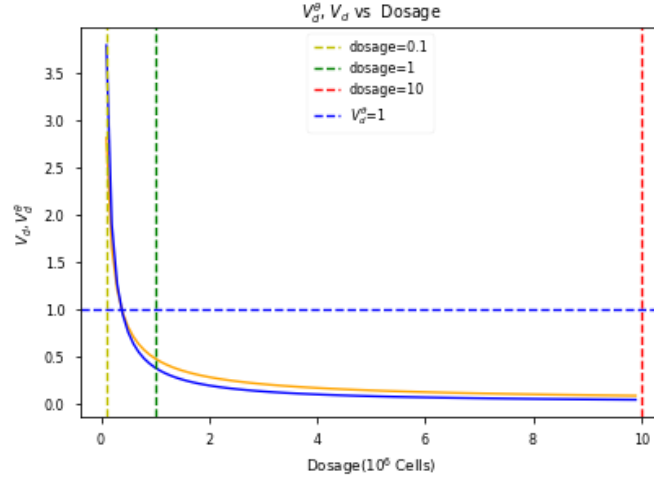


Figure 6: Plots of  $V_d$  with respect to dosages for ordinary differential model and  $V_d^\theta$  with respect to dosages for fractional order differential model.

### 3.4.1 Impact of the fractional order derivative $\theta$ to the stability of the system with small, medium and maximum dosages

We want to see how the fractional order derivative  $\theta$  affect the stability of the system. Figure 8 represents the zoom in graph of Figure 7 showing results of impact of  $\theta$  on  $V_d^\theta$  with respect to dosages closer to  $(0.5 - 2.0) 10^6$  cells.

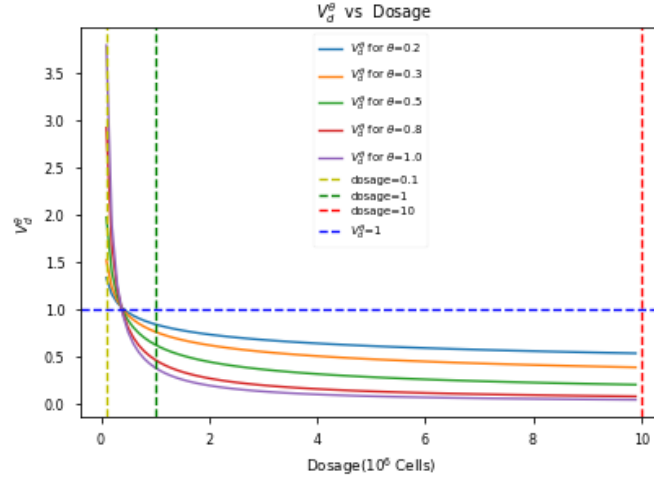


Figure 7: Impact of  $\theta$  on  $V_d$  with respect to dosages for fractional order differential model.  $V_d^\theta > 1$  for dosage and  $V_d^\theta < 1$  for medium and maximum dosages, where  $V_d^\theta = \frac{e_1^\theta k_1^\theta r^\theta}{M^* \alpha_{11}^\theta (\gamma \text{ dosage})^\theta}$ .

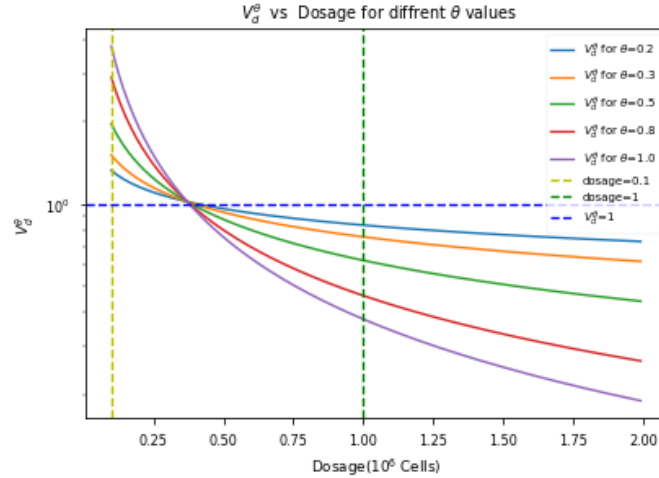


Figure 8: The zoom in graph of Figure 7 showing results of impact of  $\theta$  on  $V_d^\theta$  with respect to dosages for fractional order differential model closer to the medium dosage.  $V_d^\theta > 1$  for small dosage and  $V_d^\theta < 1$  for medium and maximum dosages, where  $V_d^\theta = \frac{e_1^\theta k_1^\theta r^\theta}{M^* \alpha_{11}^\theta (\gamma \text{ dosage})^\theta}$ .

The model (55) representing the given set of assumptions, their estimation ultimately defines the desired immunotherapy scenario, to which the model parameters are estimated

using data from [15, 19, 22, 23]. There are several numerical methods to solve fractional differential equations. In this work, We obtain the numerical solutions of prescribed model using the ABM algorithm [15, 37]. In [22] they provide scientific evidence that targeting CD70-expressing gliomas may offset the immunosuppressive effect and promote strong and sustained antitumor responses. Due to the existence of the blood- brain barrier in gliomas, they [22] claim that CAR T therapy is a superior strategy to other methods, as activated T cells are not only able to pass through the barrier but are also capable of inducing a potential antitumor response [5, 17, 29]. In [22] they illustrate that CD70 is highly expressed not only by primary tumors, but also by recurrent tumors, which presents a consistent therapeutic target for primary and recurrent gliomas. In addition, irradiation enhances CD70 expression on tumors, providing good opportunity to enhance antitumor efficacy to combine standard care with CD70 CAR therapy in glioma patients. In [22] demonstrated that CD70-specific human and murine CAR T-cells induce complete regression/improved survival in CD70+ gliomas in both xenograft and syngeneic models without toxicity. CD70 CAR T-cells “did not appear to block adaptive host immune responses” [47] and they showed in in their experiments that CD70 CAR T-cells potently induce anti-tumor reactivity against CD70+ gliomas, both in vitro and in vivo. Thus, their data suggest that CD70 may be harnessed as an immunotherapeutic target to improve outcomes in patients with gliomas. We believe our mathematical approach provides a quantitative investigating the roles of CAR T dose, immunosuppressive tumor microenvironment and individual uncertainties on the therapy response.

In Chapter 5, we discuss the sensitivity of the parameters using Sobol’s method.

## CHAPTER 4

### SENSITIVITY ANALYSIS

Sensitivity analysis allow us to quantify how the uncertainty in the output of a model is related to the uncertainty in its parameters. Performing sensitivity analysis on the model, one can identify and rank the parameters that have the greatest impact on the model output. We use Sobol's sensitivity analysis method [42], a global sensitivity analysis technique based on variance decomposition is used to quantify sensitivity of individual parameters as well as their joint effects contributing most significantly to the model output. Sobol's method measures sensitivity of the model output to model parameters with two measures: first-order sensitivity index ( $S_i$ ), and a total order sensitivity index ( $S_{T_i}$ ). first-order sensitivity index ( $S_i$ ) estimates the contribution of individual parameter to the variance in the model output, while  $S_{T_i}$  estimates the total contribution of each parameter after considering interactions with other parameters [7,20]. Parameters with first and total order sensitivity indices greater than 0.05 are considered significant to the model output [52].

#### 4.1 Sobol's Sensitivity analysis

Let us consider a mathematical model represented by a function

$$y = f(\mathbf{X}) = f(x_1, x_2, x_3, \dots, x_k),$$

where, y is the model output and  $x_1, x_2, x_3, \dots, x_k$  is the input parameters and a square integrable function  $f$  is defined in the k-dimensional unit hypercube  $\Omega^k$ ,

$$\Omega^k = \{X = (x_1, x_2, x_3, \dots, x_k) | 0 \leq x_i \leq 1; i = 1, 2, \dots, k\}.$$

The Sobol's decomposition of  $f(X)$  into summands of increasing dimension [42] given by,

$$f(x) = f_0 + \sum_{i=1}^k f_i(x_i) + \sum_i^k \sum_{i<j}^k f_{ij}(x_i, x_j) + \dots + f_{1\dots k}(x_1, \dots, x_k). \quad (60)$$

Sobol' showed that if each term in the above expansion has a zero mean, then variance decomposition of output( $V(y)$ ) can be written as follow:

$$V(y) = \int f(X^2)dX - f_0 = \sum_i^k V_i + \sum_i^k \sum_{i<j}^k V_{ij} + \sum_i^k \sum_{i<j}^k \sum_{j<l}^k V_{ijl} + \dots + V_{1\dots k}. \quad (61)$$

Sobol's sensitivity analysis measures sensitivity of the model output to model parameters with two measures: first order sensitivity index ( $S_i$ ), and the total order sensitivity index ( $S_{T_i}$ ) [43].

First order sensitivity index  $S_i$  is given by,

$$S_i = \frac{V[E(y|x_i)]}{V(y)}. \quad (62)$$

Total order sensitivity index ( $S_{T_i}$ ) is defined by,

$$S_{T_i} = 1 - \frac{V[E(y|X_{\sim i})]}{V(y)}. \quad (63)$$

where  $X_{\sim i}$  denotes all elements of X except  $x_i$

By dividing both side of the equation 61 by  $V(y)$ , respective sensitivity indices should sum up to 1.

$$\sum_i^k S_i + \sum_i^k \sum_{i<j}^k S_{ij} + \sum_i^k \sum_{i<j}^k \sum_{j<l}^k S_{ijl} + \dots + S_{123\dots k} = 1. \quad (64)$$

## CHAPTER 5

### RESULTS AND ANALYSIS

#### 5.1 ODE Model

In this chapter, the model simulates CAR T-cells treatment of gliomas. Using global sensitivity analysis, the important parameters of the ODE model are  $b_1$ ,  $\mu_T$ ,  $\mu_2$ ,  $\alpha_M$  and  $e_1$ . In mice(animal) model, tumor cells were inoculated into the brain and after some days (after  $t_1$  days, tumor burden has already undergone significant growth), mCAR T immunotherapy was administered by injection. Initial conditions for the glioma cells population were set at  $G(0)$  as the injected tumor cells,  $C_T(0) = C_M(0) = M(0) = 0$  cells and  $I_\gamma(0) = T_\beta(0) = 0 \mu$  grams. At time  $t_1$  the immunotherapy is given ( $C_T(t_1)$  is the amount of CAR T-cells).

Before we perform sensitivity analysis and model simulations, we estimated parameters  $r$ ,  $K_G$  of logistic model and parameters of  $l, d, s$  and  $w$  of Beddington DeAngelis functional response. We assume that glioma cells grows logistically with the growth rate ( $r$ ) and the carrying capacity ( $K_G$ ) in the absence of the immune system and estimate  $r$  and  $K_G$  describe in the Table 5 using the data obtained in Figure 2 by Ge *et al.* [19]. Parameters of Beddington DeAngelis functional response of CAR T-cells killing of glioma cells in Equation 3 are estimated and given in Table 6 and 7 using effector to target ratio data in the Figure 5 by Jin *et al* [22] and in the Figure 2 by Jin *et al* [23].

Parameter	Symbol	Value	Ranges.
Growth rate glioma cells	$r$	$0.4 \text{ day}^{-1}$	$ [.18, .4]$
Carrying capacity of glioma (tumor)	$K_G$	$2.3065 \times 10^6 \text{ cells}$	$ [4 \times 10^5, 6 \times 10^6]$

Table 5: Estimated parameters of growth rate ( $r$ ) and carrying capacity ( $K_G$ ) of glioma cells using data by Ge *et al.* [19].

	$d(\text{day}^{-1})$	$s$	$l$	$w$
CD70 (U87)+CTR-T cells	0.1043	0.0736	1.1378	0.3323
CD70 (U87)+hCAR-T	2.0000	0.7621	0.9352	0.2423

Table 6: The parameter estimates of  $d$ ,  $s$ ,  $l$  for hCAR T and control T-cells lysis on CD70+U87 glioma cell lines using data by Jin, L *et al* [22] and Jin, L *et al* [23].

	$d(\text{day}^{-1})$	$s$	$l$	$w$
KR70+mCAR-T	1.9310	1.0183	0.5000	0.0277
KR70+Vector T	2.0000	1.4950	1.2071	0.4616

Table 7: The parameter estimates of  $d$ ,  $s$ ,  $l$  and  $w$  for mCAR T and vector T-cells lysis on murine glioma lines KR70 using data by Jin, L *et al* [22] and Jin, L *et al* [23].

### 5.1.1 Sensitivity Analysis

We perform Sobol's sensitivity analysis method on our model to identify important parameters and their interaction to the CAR T-cells immunotherapy against glioma for mouse specific CAR T and human specific CAR T therapy scenarios. Sensitivity was determined by considering the range of each parameter limited by 20% of the reference values shown in Table 2 and sampled values from each parameter distribution. We consider two cases for this sensitivity study, using data and without using data to assess the sensitivity analysis on our model.

Sensitivity analysis performed in the absence of the data shown in Figure 9 indicate that the first order and total order sensitivity indices of the parameter  $b_1$  are the highest among other parameters in the model follow by  $\mu_T, e_1, \mu_2$  and  $\alpha_M$ . Hence,  $b_1, \mu_T, e_1, \mu_2$ , and  $\alpha_M$  are the influential parameters that contribute to the model output mostly. First order Sobol's indices with higher index values indicating significant contribution of single parameters to the model output.

Next, we performed sensitivity analysis incorporating data to explore the most important parameters in our model. Sensitivity analysis results shown in Figure 10 indicate that  $\mu_T, b_1$  and  $e_1$  are the most important parameters in the model.

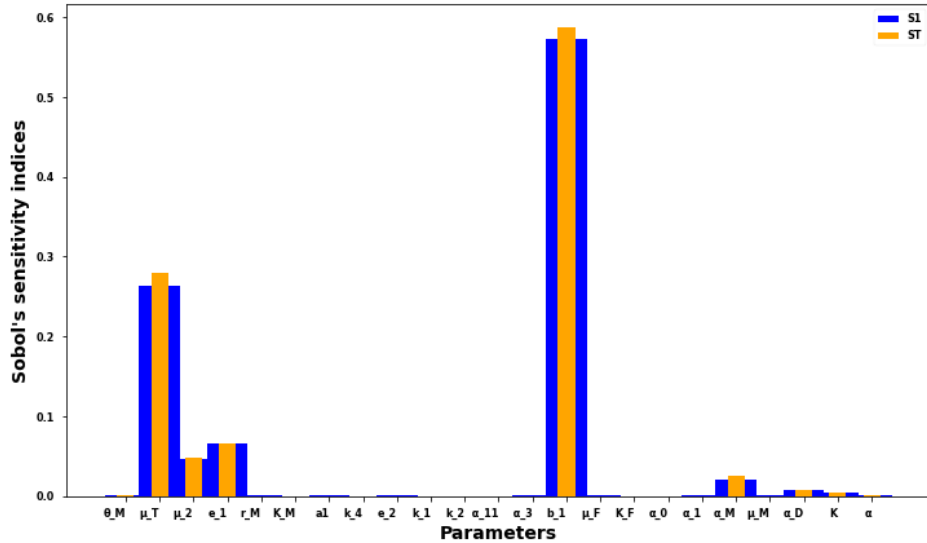


Figure 9: Sensitivity analysis in the absence of the data. Total order and first order Sobol's sensitivity indices of model parameters are shown in this graph. Total order sensitivity indices (orange bar) and first-order sensitivity indices (blue bar) are shown, respectively. The greater the sensitivity indices are, the more sensitive parameters are for the model. Both first order and total order Sobol's indices indicate that  $b_1, \mu_T, \mu_2, \alpha_M$  and  $e_1$  are the most influential model parameters.

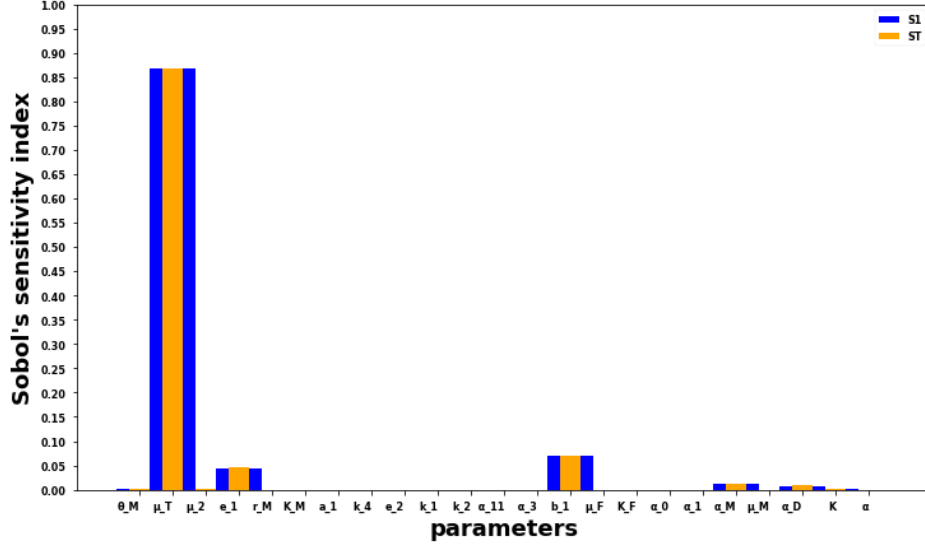


Figure 10: Sensitivity analysis using data Total order and first order Sobol's sensitivity indices of model parameters are shown in this graph. Total-order sensitivity indices (orange bar) and first-order sensitivity indices (blue bar) are shown, respectively. The results indicate that parameter  $\mu_T$  is the most important parameter of the model, followed by the important parameters  $e_1$  and  $b_1$ .

### 5.1.2 Parameter Estimation

Parameters  $\theta_M, \alpha, \mu_T, \alpha_M, \mu_2$  and  $e_1$  were estimated using the experimental data. Parameters  $r, K_G, d, s$  and  $l$  and  $w$  estimated see Table 5, 6 and 7. The remaining parameter values used in the simulations are shown in Table 2.

We determined the two equilibrium points, tumor free equilibrium point ( $E_1$ ) and the non-zero tumor equilibrium point ( $E_2$ ) of the system and the criteria for the stability of equilibrium points. Tumor free equilibrium point  $E_1$  for both hCAR T and mCAR T treatment scenarios as follow.

$$E_1 = \left( G^* = 0, C_T^* = 0, C_M^* = 0, I_\gamma^* = \frac{\alpha_0}{\mu_F}, T_\beta^* = 0, M^* = 0 \right). \quad (65)$$

Using parameter values tuning and literature, we obtain the parameter values and substi-

tute parameter values in eigenvalues of the jacobian matrix to get the following eigenvalues for hCAR T and mCAR T-cells respective dosages.

The eigenvalues of the Jacobian matrix  $J(E_1)$  about the equilibrium point  $E_1$ :

$$\left[ \frac{e_1 k_1 r - \gamma M^* \alpha_{11} \text{dosage}}{e_1 k_1}, \left( \frac{K_M - 2M^*}{K_M} \right) r_M, -\alpha_M - \mu_T, -\mu_M, -\mu_F, -\mu_2 \right].$$

Eigenvalues of tumor free equilibrium point of hCAR T for small dosage,

$$[2.5578 \times 10^{-6}, -0.7968, -0.26, -0.0450, -2.4480, -0.4090].$$

Eigenvalues of tumor free equilibrium point of hCAR T for medium dosage,

$$[-9.8174 \times 10^{-6}, -0.7968, -0.26, -0.0450, -2.4480, -0.4090].$$

Eigenvalues of tumor free equilibrium point of hCAR T for maximum dosage,

$$[-1.3357 \times 10^{-4}, -0.7968, -0.26, -0.0450, -2.4480, -0.4090].$$

## **Eigenvalues of tumor free equilibrium point of mCAR T scenario for small, medium and Maximum dosages**

Eigenvalues of tumor free equilibrium point of hCAR T for small dosage

$$[2.4847 \times 10^{-4}, -0.7968, -0.245, -0.0450, -2.4480, -0.4090].$$

Eigenvalues of tumor free equilibrium point of hCAR T for medium dosage

$$[-6.909 \times 10^{-4}, -0.7968, -0.245, -0.0450, -2.4480, -0.4090].$$

Eigenvalues of tumor free equilibrium point of hCAR T for maximum dosage

$$[-1.0448 \times 10^{-2}, -0.7968, -0.245, -0.0450, -2.4480, -0.4090].$$

Positive eigenvalues for small dosage indicate that tumor free equilibrium points for both hCAR T and mCAR T-cells scenarios are unstable. Medical point of view this means that

the tumor will grow and drive the system to explosion.

### 5.1.3 Insights on hCAR T dosing strategy into the elimination of U87 tumor

We want to assess the relationship between human CD70 specific CAR T (hCAR T) immunotherapy dose and tumor response in mouse models. We perform three different simulations with CD70 hCAR T therapy doses of small ( $1 \times 10^5$ ), medium ( $1 \times 10^6$ ) and maximum ( $1 \times 10^7$ ) cells against tumor burdens after 7 days of the inoculation of  $5 \times 10^4$  tumor cells. We consider model parameters described in Table 2 and initial tumor burden of  $G_0 = 5 \times 10^4$  cells. Figures 11-13 show that the dynamics of the three state variables, namely, malignant CD70 specific hCAR T-cells and memory CAR T-cells and glioma cells. Maximum dose of ( $1 \times 10^7$ ) cells is able to eliminate the tumor completely, higher number of CAR T-cells is able to generate greater immunological memory pool. Medium dose of CAR T-cells ( $1 \times 10^6$ ) cells applied after day 7 of tumor inoculation is able to eliminate the tumor after 10 days of immunotherapy. Finally, small dose of CAR T  $1 \times 10^5$  cells initially reduces the tumor briefly. However, it grows back to  $0.6 \times 10^6$  cells.

### 5.1.4 The number of injected hCAR T-cells does affect treatment outcome

We simulate the results of the study that were presented in Figure 6A of [22]. In the study [22], groups of mice were injected with  $5 \times 10^4$  tumor cells, then after 7 days of tumor inoculation, mice were treated with different dosages  $10^5$ ,  $10^6$ , and  $10^7$  cells of CD70 specific human CAR T immunotherapy respectively. In the study, a complete regression was seen in  $10^7$  hCAR T-cells per mouse group, an intermediate effect in  $10^6$ h CAR T-cells per mouse

group, and no effect in the  $10^5$  hCAR T-cells per mouse group in survival.

Simulations for hCAR T scenario, We consider initial condition of  $G(0) = 5 \times 10^4$  as the injected CD70 glioma cells and simulate the mathematical model with  $10^5$ ,  $10^6$ , and  $10^7$  three doses of CAR T-cell therapy after 7 days of tumor inoculation. Figures 11-13 shows simulated glioma cells, CAR T-cells and memory T-cells dynamics over time in response to the  $5 \times 10^4$  cells tumor burden and  $C_T(0) = C_M(0) = 0$  cells.

In Figure 11, Simulation begins with  $G(0) = 5 \times 10^4$  cells, and tumor grows in time until it reaches about  $0.35 \times 10^6$  cells in  $t = 7$  days. At this time, mice were exposed with small ( $10^5$  cells) dosage of CD70 hCAR T immunotherapy, which did not eliminate the tumor, tumor burden reaches about  $0.6 \times 10^6$  cells about 17 days. In Figures 12 and 13, simulations show the dynamics of memory T-cells and hCAR T for small dose of post hCAR T therapy, in which CAR T-cells does not undergo rapid growth. Memory T-cells dynamics for small dose of hCAR T in Figure 12 shows slow progression.

We simulate the CD70 hCAR T therapy of medium ( $10^6$  cells) dose against  $G(0) = 5 \times 10^4$  glioma cells. In Figure 11, Beginning with  $G(0) = 5 \times 10^4$  cells, the tumor grows rapidly and reaches about  $0.35 \times 10^6$  cells at day 7 when  $C_T = 10^6$  cells of CD 70 CAR T immunotherapy is applied, CAR T-cell therapy is able to eliminate the tumor about 32 days after CAR T therapy. Simulation results in Figure 13 shows dynamics of hCAR T-cells in which hCAR T-cells grows and reach to  $16 \times 10^6$  cells and decreases over time. Memory T-cells dynamics for medium dose of hCAR T-cells in Figure 12 shows memory T-cells grow about  $0.7 \times 10^6$  after  $10^6$  hCAR T-cells dose introduced to mice.

We reproduce  $10^7$  CD70 CAR T-cells immunotherapy against glioma cells with simulations. First, we consider  $G(0) = 5 \times 10^4$  tumor burden and after 7 days it increases about

$0.35 \times 10^6$  cells. At that time,  $C_T = 10^7$  CD70h CAR T-cells were introduced, complete tumor elimination is observed about 18 days of hCAR T-cell therapy, see Figure 11. After introduction of hCAR T-cell therapy,  $C_T$  cells grows rapidly and reach to maximum value of  $45 \times 10^6$  and decreases over time while memory T-cells undergo rapid growth, see Figure 12.

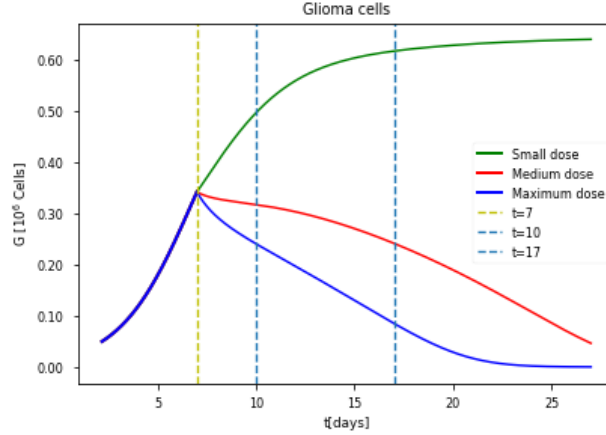


Figure 11: **Glioma cells dynamics.**  $G(0)=5 \times 10^4$  CD70 glioma cells were injected to the mice. After day 7 of tumor inoculation, Small, medium and maximum doses of hCAR T-cells is injected to the mouse respectively. Small dose of hCAR T-cells is not able to eliminate the tumor. Tumor grows and reach to  $0.6 \times 10^6$  cells. Medium dose of hCAR T-cells eliminate the tumor about 28 days after application of hCAR T-cell therapy. However, with maximum dose of hCAR T-cells, tumor elimination occurs around 5 days after injection of hCAR T-cells.

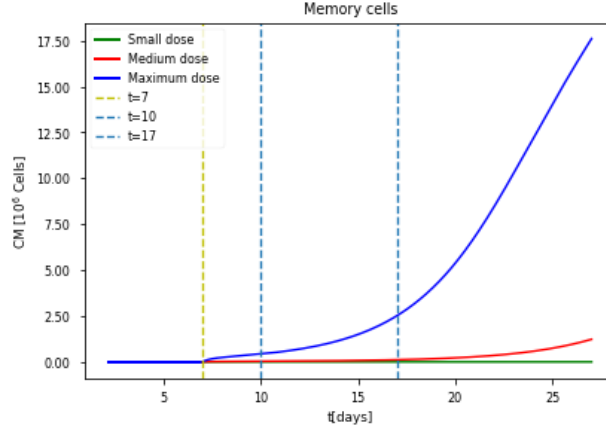


Figure 12: **Dynamics of Memory T-cells.** Beginning with  $G(0) = 5 \times 10^4$  glioma cells, when the tumor reaches about  $0.35 \times 10^6$  cells at day 7, small, medium and maximum cells doses of hCAR T-cells is introduced respectively. Memory T-cell population is formed in dose dependent manner. Higher CAR T-cells doses generate higher memory T-cells.

All our simulation results for human CD70 CAR T-cells immunotherapy scenario against glioma cells agree with the in vivo study results presented in [22] Figure 6A.

### 5.1.5 Maximum expansion of human specific CAR T-cells (hCAR T) at day 7 of injection

We see the persistence of CAR T-cells for a long time. It has been described that when the number of CAR T-cells injected is small, the therapy can fail [22]. However, the injection of low CAR T-cells numbers is typically done when these cells do not expand well in-vitro, which could be the result of a low stimulation capability. We simulated the effect of injected CAR T-cells, and the dynamics of treatment was substantially affected, see Figure 13. A reduction in dosage of the CAR T-cells led to slower growth of this population, resulting in tumor growth reaching unacceptable levels without any pre-clinical response.

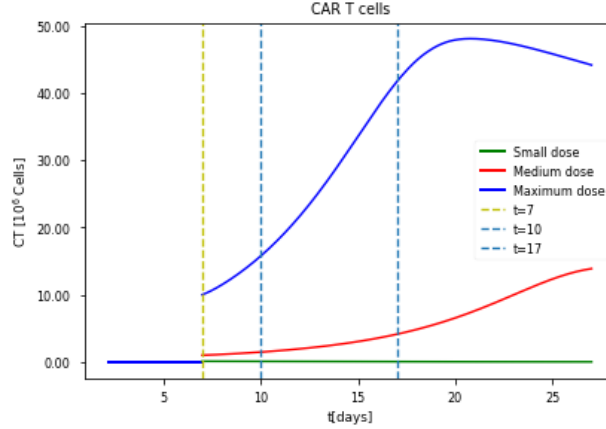


Figure 13: **Dynamics of hCAR T-cells.** Beginning with  $G(0) = 5 \times 10^4$  U87 tumor cells are introduced, when tumor reaches about  $0.35 \times 10^6$  cells after day 7, small, medium and maximum dose of hCAR T-cells are introduced. CAR T-cells grows and then gradually decrease over time.

### 5.1.6 Insights on mCAR T dosing strategy into the elimination of KR70 tumor

We want to explore the relationship between mouse CD70 specific CAR T immunotherapy dose and tumor response in mouse models after 5, 7, 8 and 18 days of tumor inoculation. Due to the heterogeneous nature of the glioma cells, we consider two types of tumors namely KR70-C and KR70-B. We perform three different simulations with CD70 CAR T therapy doses of small ( $1 \times 10^5$ ), medium ( $1 \times 10^6$ ) and large ( $1 \times 10^7$ ) cells against tumor burdens. The cells, model parameters are described in Table 2 and initial tumor burden of glioma cells,  $G_0 = 1 \times 10^5$  cells. Figures 15- 14 show the dynamics of the three state variables, namely, CD70 specific CAR T-cells and memory CAR T-cells and malignant glioma cells respectively. Immunotherapy of mCAR T is applied separately after 5, 7, 8 and 18 days of tumor inoculation, Large dose of ( $1 \times 10^7$ ) cells is able to eliminate the tumor completely, higher number of CAR T-cells is able to generate greater immunological memory pool. Although,

Medium dose of CAR T-cells ( $1 \times 10^6$ ) cells applied after day 5 of tumor inoculation is able to eliminate the tumor, same dose of CAR T-cells performed after 7 of tumor implantation is not able to eliminate it. It decrease but resumes growth to equilibrium state. Finally, small dose of CAR T  $1 \times 10^5$  cells initially reduces the the tumor. However, it grows back for day 5 or day 7 of CAR T-cells immunotherapy.

### **5.1.7 The number of injected mouse specific CD70 CAR T-cells does affect treatment outcome**

We want to reproduce the scenarios described in Figures 6B and 6C of [22] with simulations.

In the Figure 14, Beginning with  $G(0) = 1 \times 10^5$  KR70 tumor cells are introduced, when tumor reaches about  $0.35 \times 10^6$  cells after day 5, we performed  $C_T = 1 \times 10^5$  small dose of CD70 specific mouse CAR T (mCAR T) cells, which reduced the tumor briefly. Then grow rapidly until it reaches around  $0.6 \times 10^6$  cells. See Figure 14.

For the medium dose, simulation begins with  $G(0) = 1 \times 10^5$  KR70 tumor cells, and tumor progresses until it reaches about  $0.35 \times 10^6$  cells in 5 days, At this time,  $C_T = 1 \times 10^6$  of CD70 specific mouse CAR T (mCAR T) cells T is performed, it eliminate the tumor about 19 days of CAR T-cell therapy. For the Maximum dose, simulation begins with  $G(0) = 1 \times 10^5$  KR70 tumor cells, it grows rapidly about  $0.35 \times 10^6$  cells in 5 days. at that time Maximum dose of  $C_T = 1 \times 10^7$  were performed, it eliminates the tumor about 8 days of CAR T-cell therapy, see Figure 14.

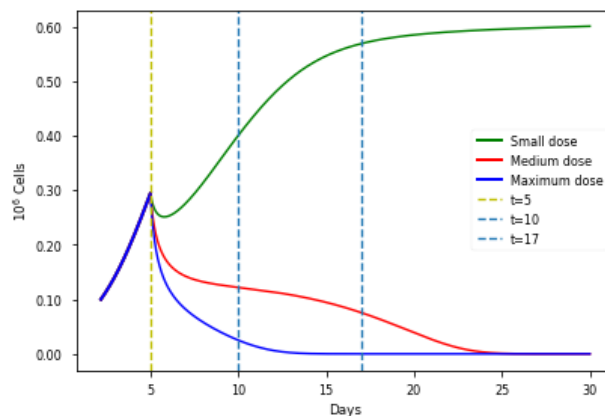


Figure 14: **Dynamics of Glioma cells.** Initial CD70 glioma cells of  $G(0) = 1 \times 10^5$  were injected to the mice. After day 5 of tumor inoculation, small, medium and maximum doses of mCAR T-cells is injected to the mouse respectively. Small dose of mCAR T-cells is not able to eliminate the tumor. Tumor grows and reach to  $0.6 \times 10^6$  cells. Medium dose of mCAR T-cells eliminate the tumor about 25 days after application of CAR T-cell therapy. However, with maximum dose of CAR T-cells, tumor elimination occurs about 8 days after injection of CAR T-cells.

### 5.1.8 Maximum expansion of mouse specific CAR T-cells (mCAR T) at day 5 of injection

Beginning with  $G(0) = 1 \times 10^5$  KR70 tumor cells are introduced, when tumor reaches about  $0.35 \times 10^6$  cells after day 5, small, medium and maximum dose of mCAR T-cells are introduced. CAR T-cells grows and then gradually decrease over time. For the medium and small dose of mCAR T-cells, CAR T-cells decreases over the time [see Figure15]. Memory T-cells population is formed in dose dependent manner. Higher CAR T-cells doses generate higher memory T-cells and higher CAR T-cells doses generate higher memory T-cells, see Figure 16.

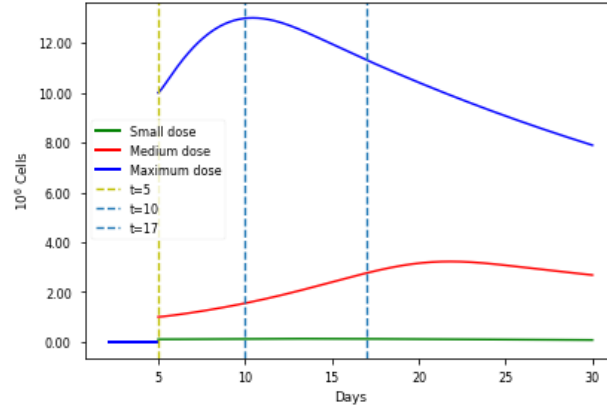


Figure 15: **Dynamics of mCAR T-cells.** Beginning with  $G(0) = 1 \times 10^5$  KR70 tumor cells are introduced, when tumor reaches about  $0.35 \times 10^6$  cells after day 5, small, medium and maximum dose of mCAR T-cells are introduced. CAR T-cells grows and then gradually decrease over time. For the medium and small dose of mCAR T-cells, CAR T-cells decreases over the time.

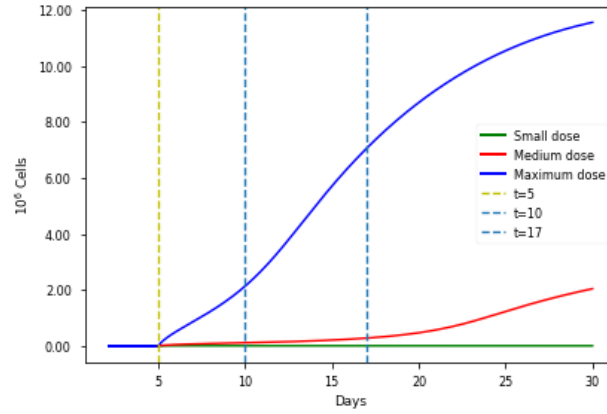


Figure 16: **Dynamics of Memory T-cells.** Beginning with  $G(0) = 1 \times 10^5$  glioma cells, when the tumor reaches about  $0.35 \times 10^6$  cells at day 5, small, medium and maximum cells doses of mCAR T-cells is introduced respectively. memory T-cells population is formed in dose dependent manner. Higher CAR T-cells doses generate higher memory T-cells.

## 5.2 FODE Model

### 5.2.1 Sobol's sensitivity analysis method

We present numerical simulations based on the parameters base values in Table 2. We use sensitivity analysis to identify the model parameters that have the most influence on the tumor compartment. It consequently provides useful insight into which model parameters contribute most to the variability of the dynamics of glioma under CAR T-cells treatment. We perform a global sensitivity analysis of our model. Then, we use global sensitivity analysis, Sobol's Method. In the absence of information that characterizes the uncertainties in the parameters of the model in Table 2, we assume that each parameter is a random variable with uniform distribution in the range limited by 20% of the reference values indicated in Table 2.

The main goal of sensitivity analysis of a glioma model is to investigate the dominant factors associated with CAR T-cells treatment that affects the glioma dynamics greatly. The analysis will determine the parameters that play an essential role in contributing to variations in the outcome of glioma cells dynamics. We do the sensitivity analysis by using the techniques as a combination of Saltelli sampling and the Sobol's method to find out the associated factors that are considered to be influential. The Sobol's technique is considered to be a reliable and efficient method in order to measure monotonic and nonlinear association among inputs and output results in the model. The sensitivity analysis gives the scaled Sobol's sensitivity index and the total scaled sensitivity index, by which one can determine the uncertainty level in the glioma model. The most dominant parameters associated with our glioma model are to be those that have high Sobol's indices values. Parameters with

sensitivity indices greater than 0.05 are considered significant [52]. We seek parameters which are sensitivity analysis of dynamics of glioma under CAR T-cells treatment to identify the influence of the model parameters on the solutions for (a) CAR T-cells, and (b) glioma tumor cells. The Sobol’ sensitivity indices are shown as bar-graph in Figure 17. It can be observed from Table 2, that the most sensitive parameter is  $\alpha_M$  with the high scaled Sobol’ index followed by  $b_1$  and  $\mu_2$ .

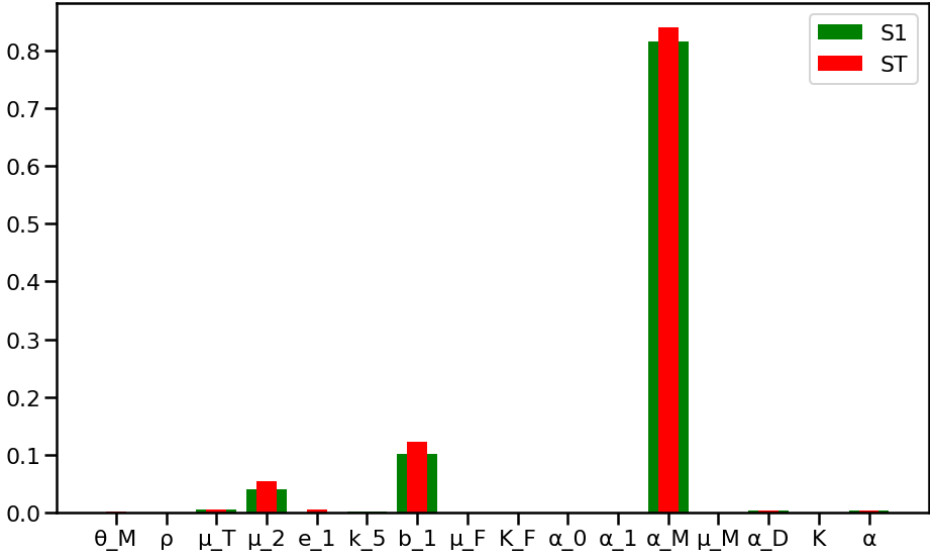


Figure 17: Sensitivity analysis (FODE model). Sensitivity analysis of a system to identify the influence of the model parameters on the solutions for (a) CAR T-cells, (b) glioma tumor cells. We use scaled Sobol’s sensitivity to rank sensitivity to the dynamics  $G$  cells population. The immune-therapy with mCAR T on CD70+KR70 dosage ranging from 0.1 to 10 [ $10^6$  mCAR T-cells]. CAR T-cells after 7 days implantation of the tumor  $G(0) = 1 \times 10^5$ .

Table 8: Sobol's Method

Parameters	Definitions	$S_1$	$S_T$
$e_1$	Michaelis Menten constant	0.060	0.176
$k_5$	Inhibitory parameter	0.000	0.000
$\alpha_D$	killing rate of glioma cells by $C_T$ cells	0.000	0.000
$K$	Half saturation constant	0.000	0.000
$\mu_T$	Death rate of $C_T$ cells	0.001	0.000
$\theta_M$	Rate of change of $C_M$ to $C_T$	0.000	0.000
$\alpha$	Rate of inhibition of glioma cells by $C_T$ cells	0.000	0.000
$\alpha_M$	Rate of differentiation of $C_T$ in to $C_M$	0.026	0.065
$\mu_M$	Death rate of $C_M$	0.000	0.000
$\alpha_0$	Constant source of <i>interferon</i> $_\gamma$	0.000	0.000
$\alpha_1$	Rate of activation of <i>interferon</i> $_\gamma$ by $C_T$ cells	0.000	0.000
$K_F$	Half-saturation constant	0.000	0.000
$\mu_F$	degradation rate of <i>interferon</i> $_\gamma$	0.000	0.000
$b_1$	release rate per glioma cells	0.12	0.19
$\mu_2$	degradation of $T_\beta$	0.033	0.075

Model parameters sensitivity with initial conditions,  $G(0) = 0.44[10^6 \text{ cells}]$ ,  $C_T[0] = 10[10^6 \text{ cells}]$ ,  $C_M(0) = 0, F(0) = 0, T_\beta(0) = 0$   $S_1$  is first order Sobol's index and  $S_T$  is total order Sobol's index.

In this section, we use a system of fractional order ordinary differential equations model (55) to simulate the scenarios of both human and mouse CARs in xenograft and syngeneic orthotopic glioma models. For human CAR (hCAR) T cells, various doses ( $10^5 - 10^7$ ) per mouse were adoptively transferred into tumor-bearing mice 7 days after tumor inoculation [22]. We assume that the mice lacked major immune cells components [22]. We also simulate a mouse version (mCAR) in syngeneic mice. We incorporate heterogeneous gliomas by simulating:

1. Tumors derived from a single clone of a CD70+glioma cell line KR70-C.
2. Bulk tumors, KR70-B

We simulate them for 17 days. We estimate a few of the most uncertain parameters, report

model predictions of anti-tumor response of CD70 CAR T-cells against CD70+gliomas.

### 5.2.2 Model fitting to experimental data

We fit a small number of the model parameters,  $\theta_M, \alpha, \alpha_M, \mu_2, e_1$ , and  $\mu_T$ , to CAR T-cells data using a least squared error scheme. The data for fitting is from [23] (see Figure 2C).

Our model tracks down the dynamics of gliomas and CAR T-cells as follows:

1. In the first simulations, the model tracks down the number of gliomas cells for seven days after inoculation of  $5 \times 10^4$  glioma cells (CD70+U87) with zero dosage of hCAR T-cells administered.
2. Then after seven days the model tracks down glioma, hCAR T-cells, memory hCAR T-cells after various doses ranging from  $10^5$  to  $10^7$  hCAR T-cells have been administered on the seventh day.
3. In the second simulations, the model tracks down the number of KR70 tumor cells (derived from a tumor clone we denote these cells by KR70-C) for five or seven days after inoculation of  $1 \times 10^5$  glioma cells with zero dosage of CAR T-cells administered.
4. Then after five or seven days the model tracks down glioma, CAR T-cells, memory CAR T-cells after maximum dose  $10^7$  NT or CAR T-cells have been administered on the fifth or seventh day. The simulations at day 10 and day 17 after the maximum dose has been administered were compared to preclinical studies in [22].
5. In the third simulations, the model tracks down the number of KR70-B tumor cells (bulk KR70 cells) for eight or eighteen days after inoculation of  $1 \times 10^5$  glioma cells

with zero dosage of CAR T-cells administered.

6. Then after eight or eighteen days the model tracks down glioma, CAR T-cells, memory CAR T-cells after maximum dose  $10^7$ mCAR T-cells have been administered on the eighth or eighteenth day. The simulations were tracked down at day 8 and day 18 after the maximum dose has been administered to compare to preclinical studies in [22].

For all simulations, the initial conditions are found in Table 3. In Figure 18, we plot the simulated CAR T-cells data, starting from the initial inoculation of CAR T-cells in mice for 25 days, alongside the empirical data. Although towards the end CAR T-cells seems to drop but seems to show up trend, this is okay eventually CAR T-cells will drop. Our simulations show that the model provides a reasonable fit of the empirical data. All model parameters values (both fit and estimated) can be found in Table 5, along with references and estimated biological range. Initial baseline values are listed in Table 3.

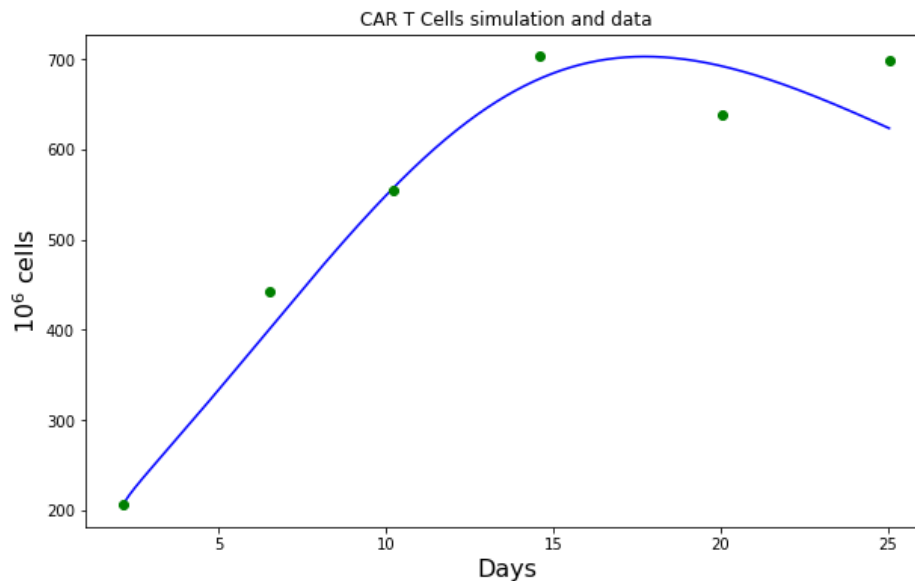


Figure 18: Model fit to CAR T-cells data. The  $x$ -axis is the number of days since the inoculation of the tumor, and the  $y$ -axis is the number of CAR T-cells (unit is  $10^6$  cells). The dotted graph represents data of CAR T-cells of Figure 2c in [23]. The curve is the simulated number of CAR T-cells.

In Figure 18, we plot the simulated CAR T-cells data, starting from the initial inoculation of CAR T-cells in mice for 25 days, alongside the empirical data. Although towards the end CAR T-cells seems to dip but seems to show up trend, this is okay eventually CAR T-cells will dip. Our simulations show that the model provides a reasonable fit of the empirical data.

All model parameters values (both fit and estimated) can be found in Table 2, along with references and estimated biological range.

### 5.2.3 The impact of inoculation of CAR T-cells on the tumor progression human xenograft glioma model

We examine the model-predicted response to the human CARs and non transduced T cells treatments in human xenograft models. For hCAR, various doses ( $10^5$ – $10^7$  per mouse) of the hCAR T-cells were transferred into tumor-bearing mice 7 days after tumor inoculation. The simulation of the dynamics of glioma cells, see (Figure 19), shows that glioma cells are completely eliminated after 17 days with medium and maximum doses treatment. The maximum dose treatment eliminates the glioma cells at the faster rate than the medium dose treatment. The small dose treatment has effect tumor, we see glioma cells increases during this period of seven days. For NT T, various doses ( $10^5$ – $10^7$  per mouse) of the NT T cells were transferred into tumor-bearing mice 7 days after tumor inoculation, but the simulation of the dynamics of glioma cells, see (Figure 25), has no effect on the tumor, infact for all three doses treatments we see that glioma cells increases during 17 days period. Treatment with hCAR T-cells the maximum dose treatment has the highest levels of immune stimulating factor see (Figure 22) but lowest level of immune inhibiting factor (Figure 23). For simulations of the dynamics of hCAR T-cells, see (figure 20), and memory hCAR T-cells, see (Figure 21). The simulation of recruitment of microphage dynamics, see (Figure 24).

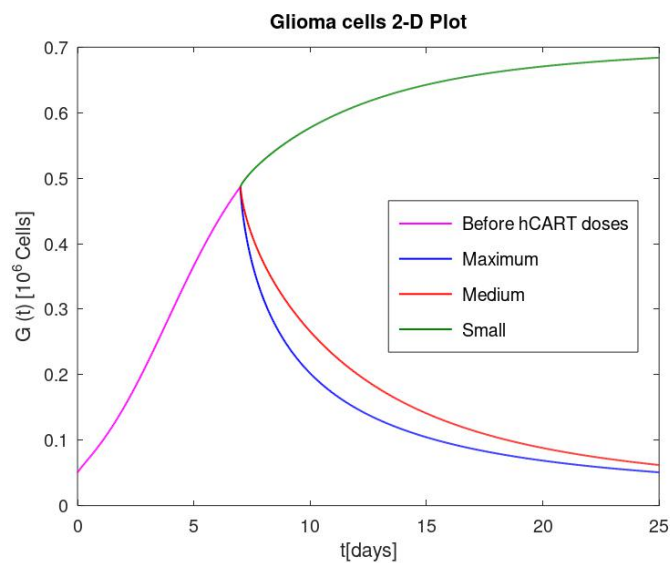


Figure 19: Glioma cells dynamics for FODE model.  $G(0) = 5 \times 10^4$  CD70 glioma cells were injected to the mice. After day 7 of tumor inoculation, Small, medium and maximum doses of hCAR T-cells is injected to the mouse respectively. Small dose of CAR T-cells are not able to eliminate the tumor.

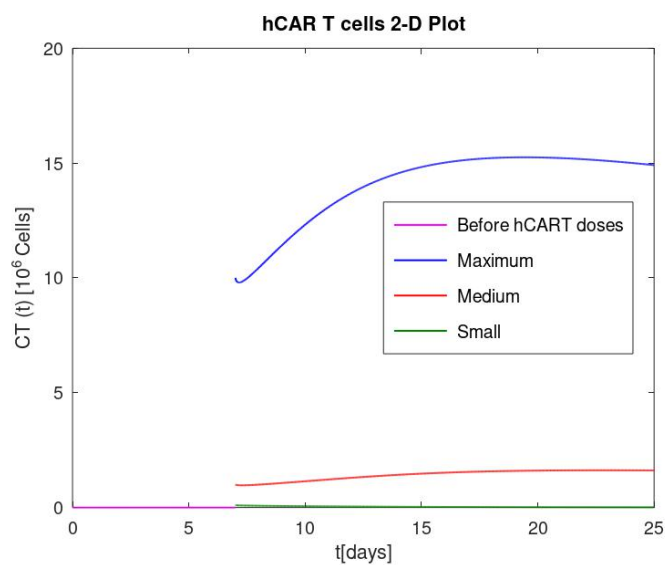


Figure 20: Dynamics of hCAR T-cells with small, medium and maximum doses treatment of hCAR T-cells.

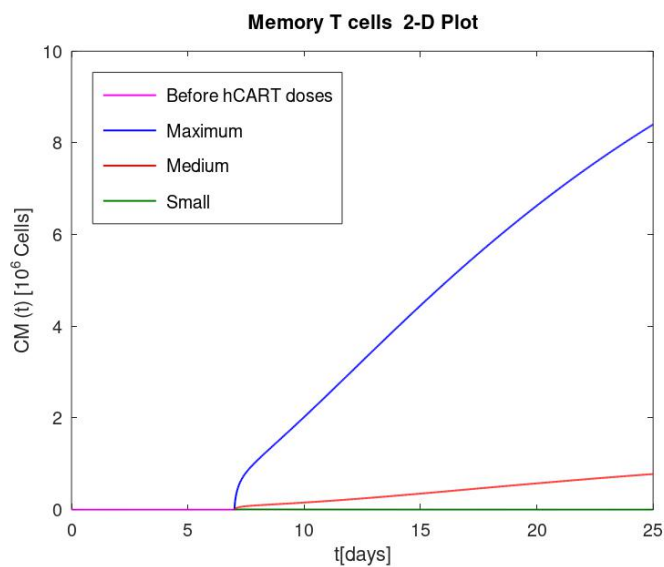


Figure 21: Dynamics of memory hCAR T-cells with small, medium and maximum doses of treatment of hCAR T-cells (FODE model).

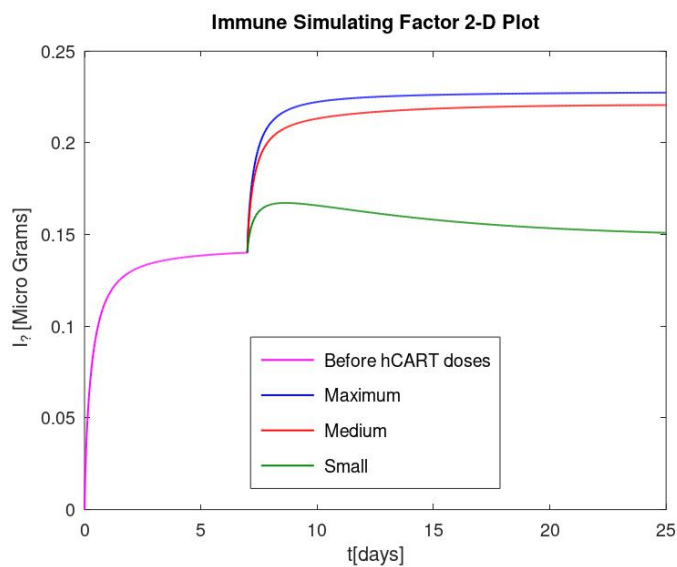


Figure 22: Dynamics of immune stimulating factor with maximum dose of treatment of hCAR T-cells.

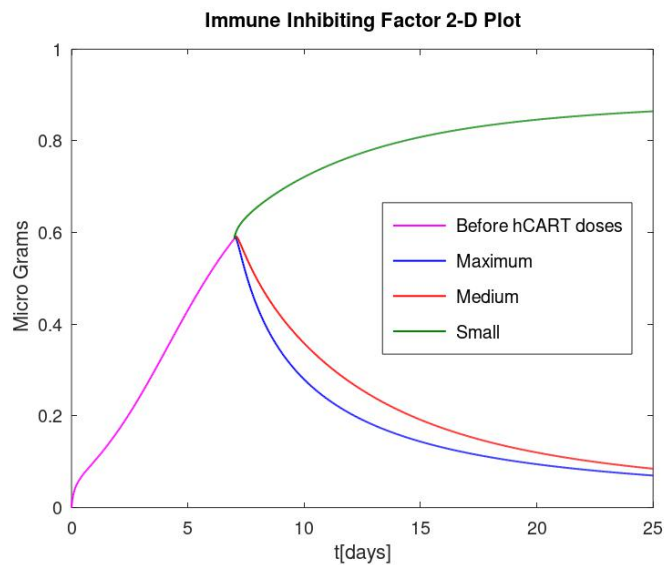


Figure 23: Dynamics of immune inhibitor factor with small, medium, and maximum doses treatment of hCAR T-cells.

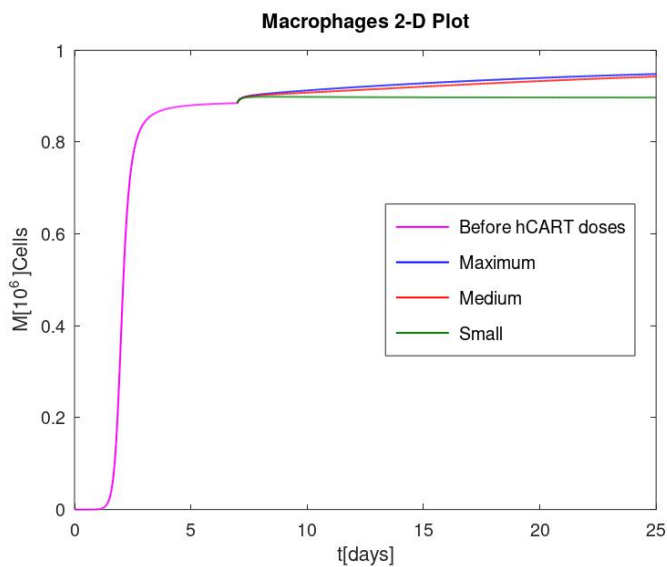


Figure 24: Dynamics of macrophages with maximum dose ( $10^7$  cells) of treatment of hCAR T-cells.

During the first few days simulated, in maximum dosage treatment CAR T-cells expanded evidencing a peak at about a few days post-injection, before their numbers stabilized and start decreasing. Both the tumor and CAR T compartments experienced a continuous

decrease towards undetectable values representing the dynamics of a mouse without residual disease (Figure 19). The lower the dosage the peaks of the CAR T compartments take longer to occur (Figures 20). We compare glioma, hCAR T and memory CAR T-cells dynamics for ODE model and FODE model respectively. See Figures 29, 30 and 31.

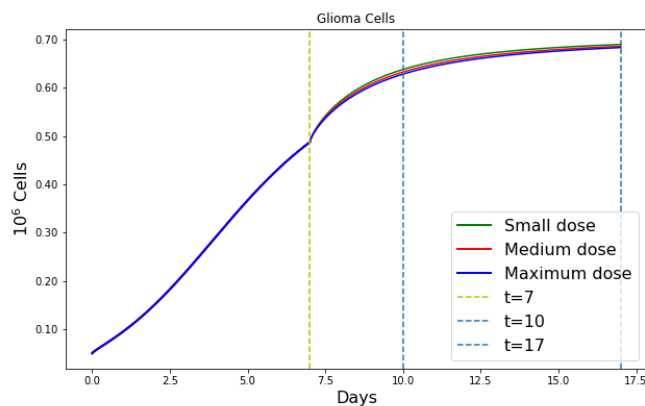
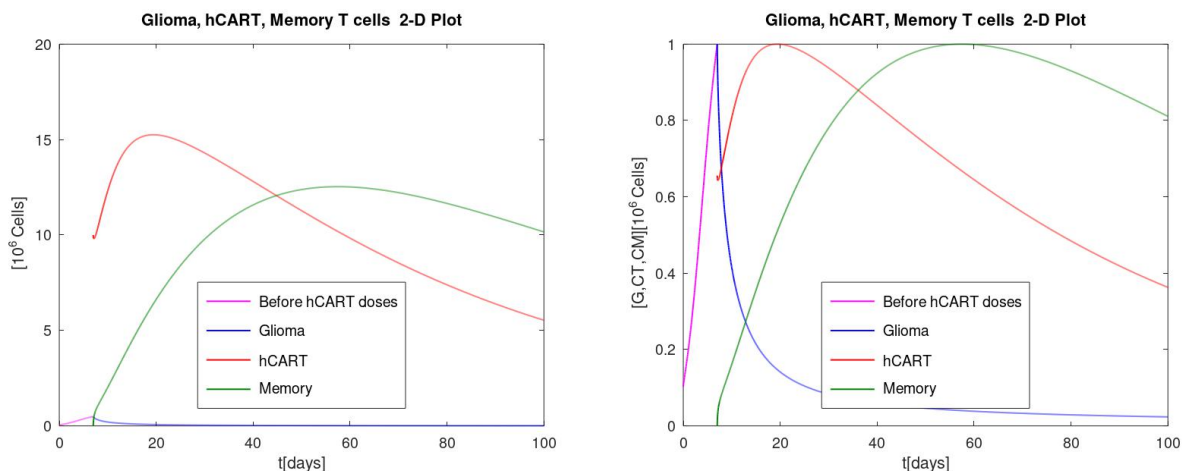


Figure 25: Dynamics of glioma with small, medium and maximum doses of NT T-cells treatment.

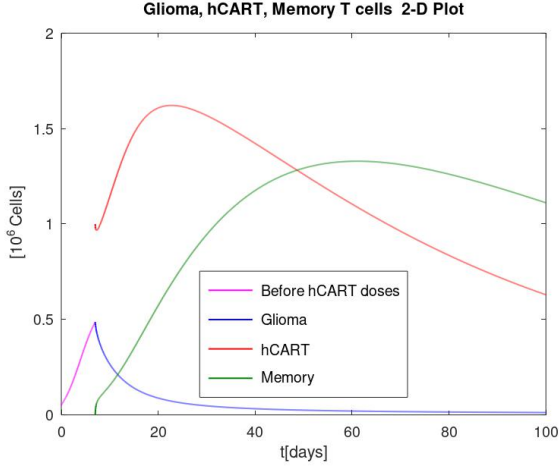


(a) Dynamics of Glioma, hCAR T and memory cells compartments with maximum treatment observed for first 100 days.

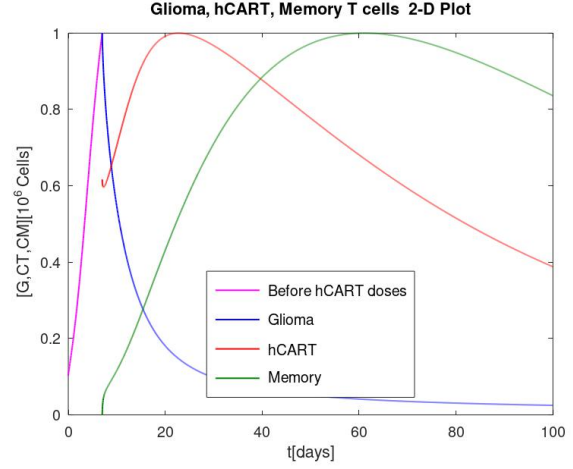
(b) Normalized plot of dynamics of Glioma, hCAR T and memory T-cells compartments with maximum treatment observed for first 100 days.

Figure 26: Dynamics of Glioma, hCAR T and memory T-cells compartments with maximum treatment observed for first 100 days for FODE model.

The expansion of the CAR T populations was increasing by several orders of magnitude compared to glioma compartment.

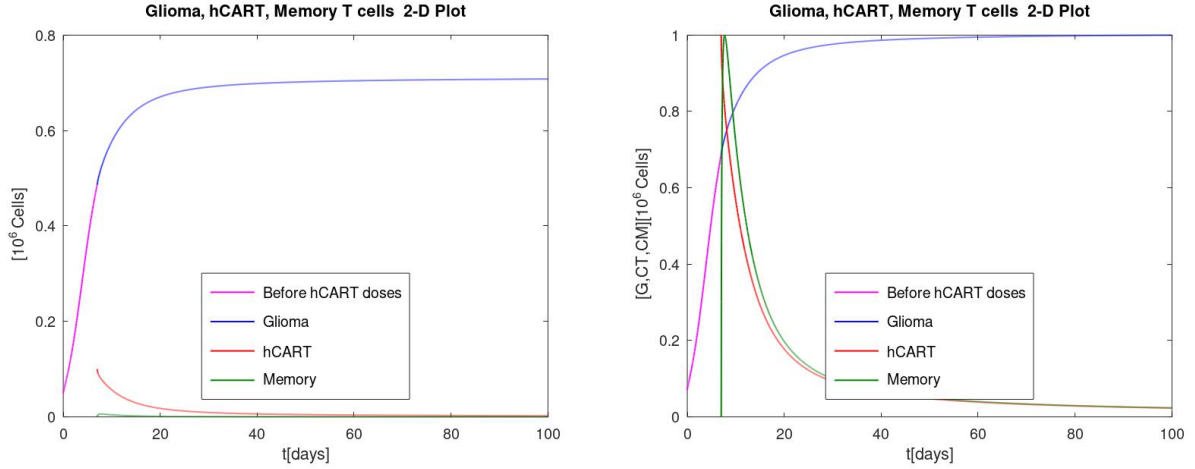


(a) Dynamics of Glioma, hCAR T and memory cells compartments with medium treatment observed for first 100 days.



(b) Normalized plot of dynamics of Glioma, hCAR T and memory T-cells compartments with medium treatment observed for first 100 days.

Figure 27: Dynamics of Glioma, hCAR T and memory T-cells compartments with medium treatment observed for first 100 days for FODE model.

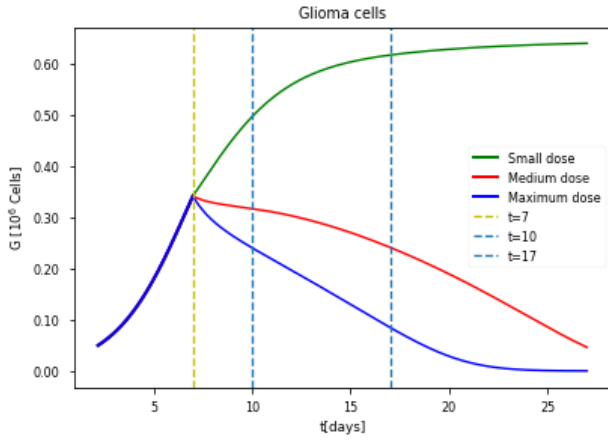


(a) Dynamics of Glioma, hCAR T and memory cells compartments with small treatment observed for first 100 days.

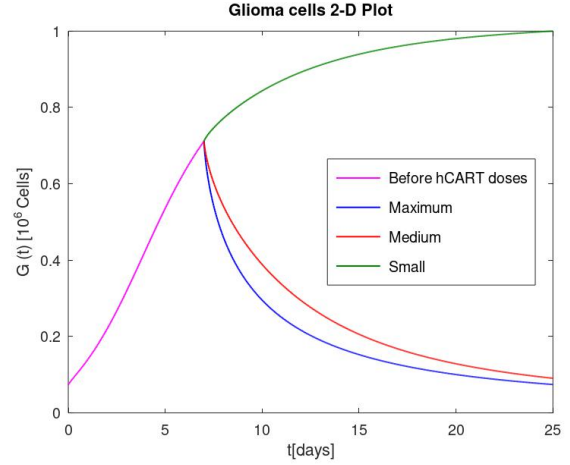
(b) Normalized plot of dynamics of Glioma, hCAR T and memory T-cells compartments with small treatment observed for first 100 days.

Figure 28: Dynamics of Glioma, hCAR T and memory T-cells compartments with small treatment observed for first 100 days for FODE model.

In summary, the model predicts preclinical studies [22] that it takes longer for medium and low dosage compared to maximum dose to eliminate glioma cells. The preclinical studies [22] studies showed that the maximum dose treatment eliminates the glioma cells in 17 days of treatment with hCAR T-cells.

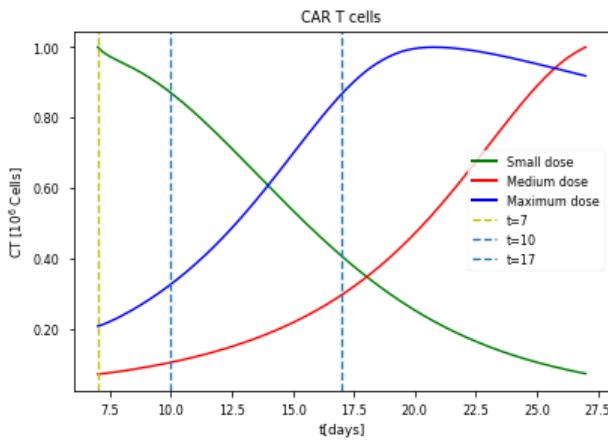


(a) Glioma cells dynamics for ODE model.

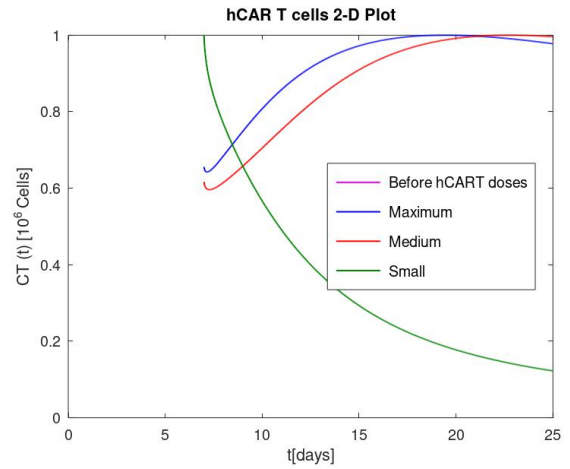


(b) Glioma cells dynamics for FODE model.

Figure 29: Glioma cells dynamics for ODE model and FODE model.

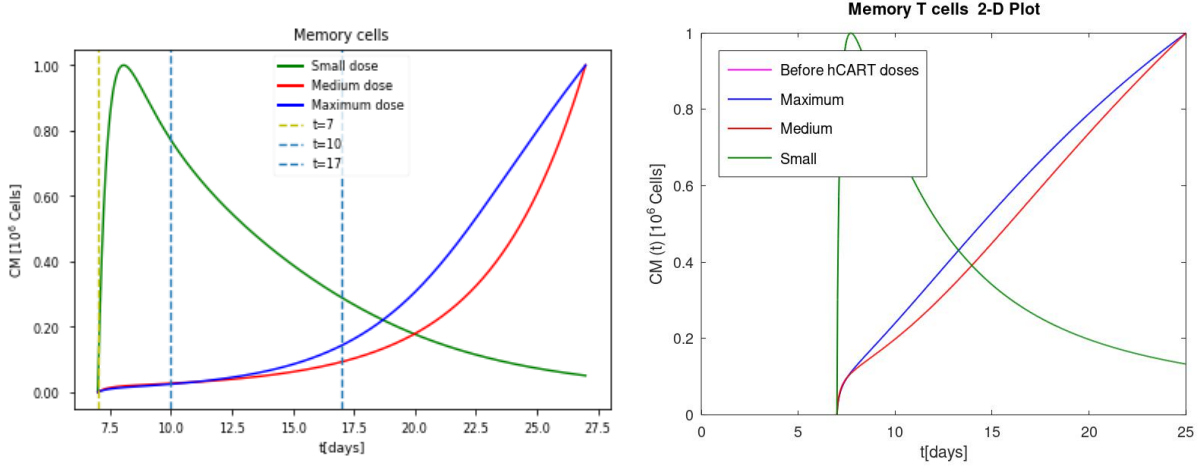


(a) hCAR T-cells dynamics for ODE model.



(b) hCAR T-cells dynamics for ODE model.

Figure 30: hCAR T-cells dynamics for ODE model and FODE model.



(a) memory T-cells dynamics for ODE model. (b) memory T-cells dynamics for FODE model.

Figure 31: Memory CAR T-cells dynamics for ODE model and FODE model.

#### 5.2.4 The impact of inoculation of non transduced (NT) T or mCAR T-cells on the KR70-C tumor progression in syngeneic glioma models

In the first set of simulations, we assume the mice were intracranially inoculated with  $1 \times 10^5$  KR70 tumor cells derived from a tumor clone, designated as KR70-C, and then adoptively transferred maximum dose of ( $1 \times 10^7$ ) NT T cells on days 5 and 7 post tumor implantation. The second set of simulations, we assume the mice were intracranially inoculated with  $1 \times 10^5$  KR70 tumor cells derived from a tumor clone, designated as KR70-C, and then adoptively transferred ( $1 \times 10^7$ )mCAR T-cells on days 5 and 7 post tumor implantation. We observe the tumor progression on the 10th day and 17th day days after the tumor implantation.

In Figures 32 and 33, illustrates that the less the tumor burden the more quickly the tumor is eliminated.

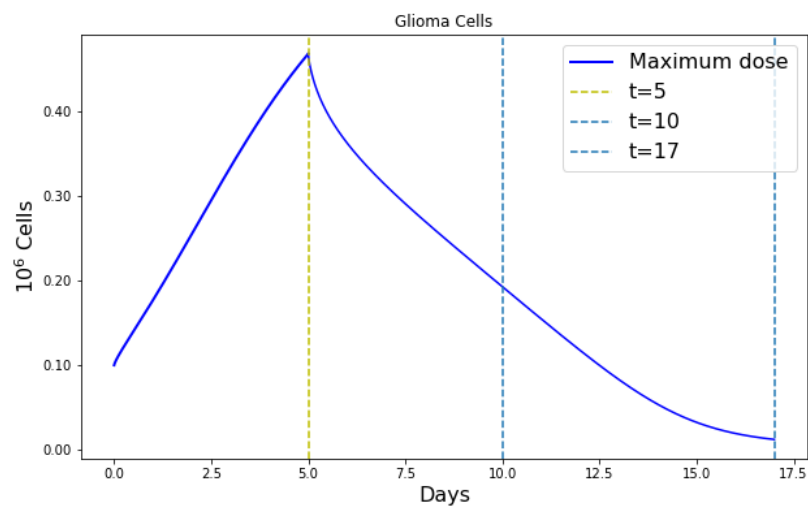


Figure 32: Dynamics of glioma compartment without treatment for the five days after inoculation of  $10^5$  of mCAR T-cells and then treated with maximum dose of  $10^7$  mCAR T-cells treatment. The mice were intracranially inoculated with  $1 \times 10^5$  KR70 tumor cells derived from a tumor clone, designated as KR70-C, and then adoptively transferred ( $1 \times 10^7$ ) mCAR T-cells on day 5 tumor implantation. Observations on progression of the glioma days 10 and 17 to compare to experimental results [22]. The simulations were inline with experimental results

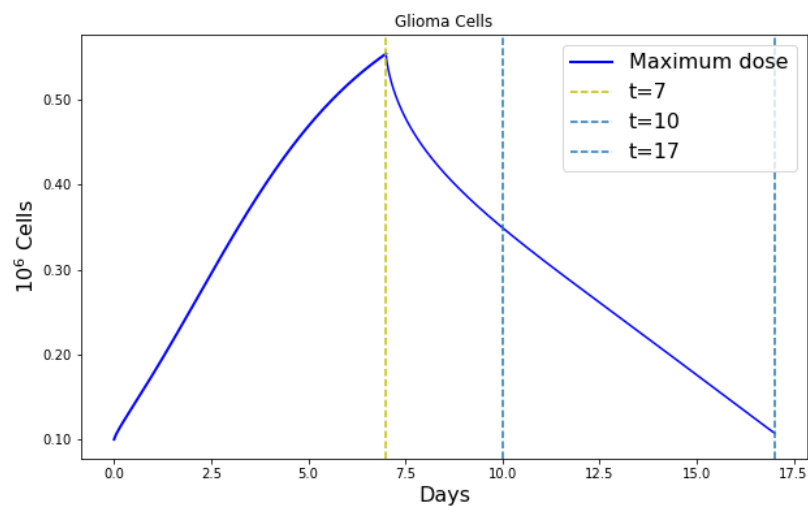


Figure 33: Dynamics of glioma compartment without treatment for the seven days after inoculation of  $10^5$  of mCAR T-cells and then treated with maximum dose of  $10^7$  mCAR T-cells treatment. The mice were intracranially inoculated with  $1 \times 10^5$  KR70 tumor cells derived from a tumor clone, designated as KR70-C, and then adoptively transferred ( $1 \times 10^7$ ) mCAR T-cells on day 7 tumor implantation. Observations on progression of the glioma days 10 and 17 to compare to experimental results [22]. The simulations were inline with experimental results.

### 5.2.5 The impact of inoculation of non transduced (NT) T or mCAR T-cells on KR70-B tumor progression in syngeneic glioma models

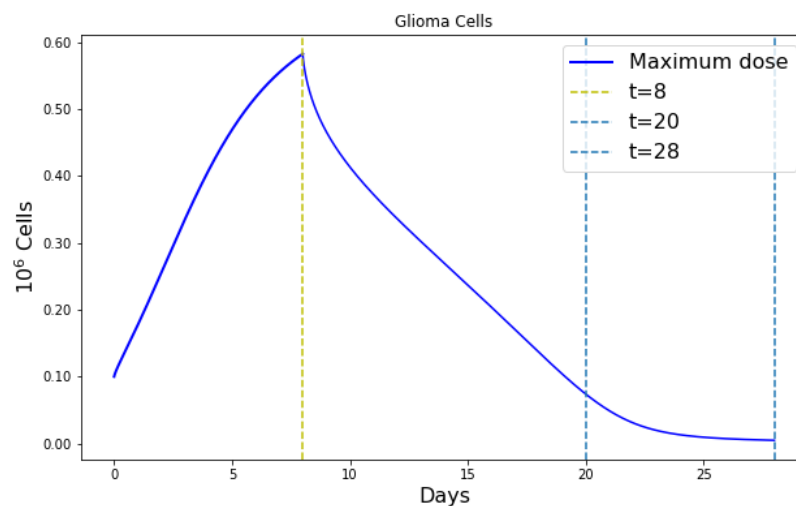


Figure 34: Dynamics of glioma compartment without treatment for the five days after inoculation of  $10^5$  of mCAR T-cells and then treated with maximum dose of  $10^7$  mCAR T-cells treatment. The mice were intracranially inoculated with  $1 \times 10^5$  KR70 tumor cells derived from a tumor clone, designated as KR70-C, and then adoptively transferred ( $1 \times 10^7$ ) mCAR T-cells on day 8 tumor implantation. Observations on progression of the glioma days 20 and 28 to compare to experimental results [22]. The simulations were inline with experimental results

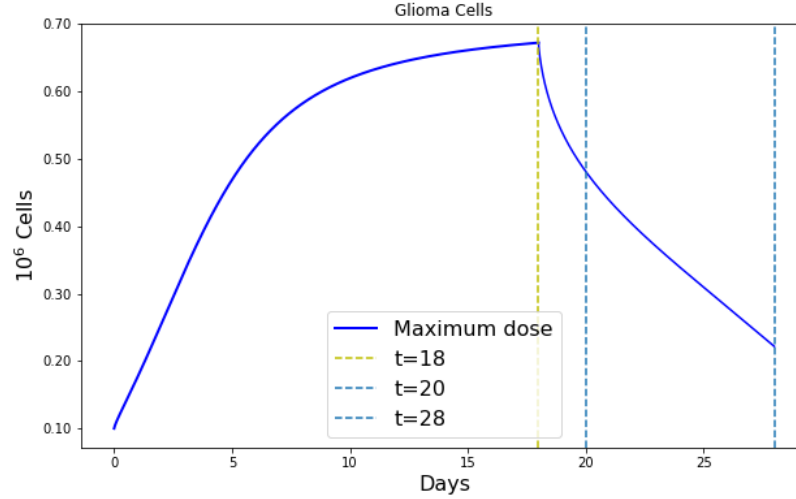


Figure 35: Dynamics of glioma compartment without treatment for the seven days after inoculation of  $10^5$  of mCAR T-cells and then treated with maximum dose of  $10^7$  mCAR T-cells treatment. The mice were intracranially inoculated with  $1 \times 10^5$  KR70 tumor cells derived from a tumor clone, designated as KR70-C, and then adoptively transferred ( $1 \times 10^7$ ) mCAR T-cells on day 18 tumor implantation. Observations on progression of the glioma days 20 and 28 to compare to experimental results [22]. The simulations were inline with experimental results.

By looking at Figures 34 and 35, the simulations supports that the more the tumor burden the longer it takes to eliminate the tumor.

### 5.2.6 The comparison of the impact of inoculation of mCAR T-cells on tumor progression in syngeneic glioma models using ODE and FODE models

We compare the simulation results of tumor progression when maximum dose of ( $1 \times 10^7$ ) mCAR T cell therapy were introduced to the mice on days 5 and 7 post tumor implantation from KR70 tumor cells derived from a tumor clone, named as KR70-C and then, maximum dose of ( $1 \times 10^7$ ) mCAR T cell therapy were introduced to the mice on days 8 and 18 post

tumor implantation from bulk tumor named as KR70-B with ODE model and FODE model. Our simulation results from both ODE and FODE models (Figures 36(a), 36(b), 36(e) and 36(f)) show that when tumor burden is less, mCAR T-cell therapy is able to eliminate the tumor burden. However, mCAR T cell therapy is not able to eliminate the tumor burden when it is large in ODE model (In Figure 36(c) and 36(d)) whereas mCAR T cell therapy clears large tumor burden in FODE model.

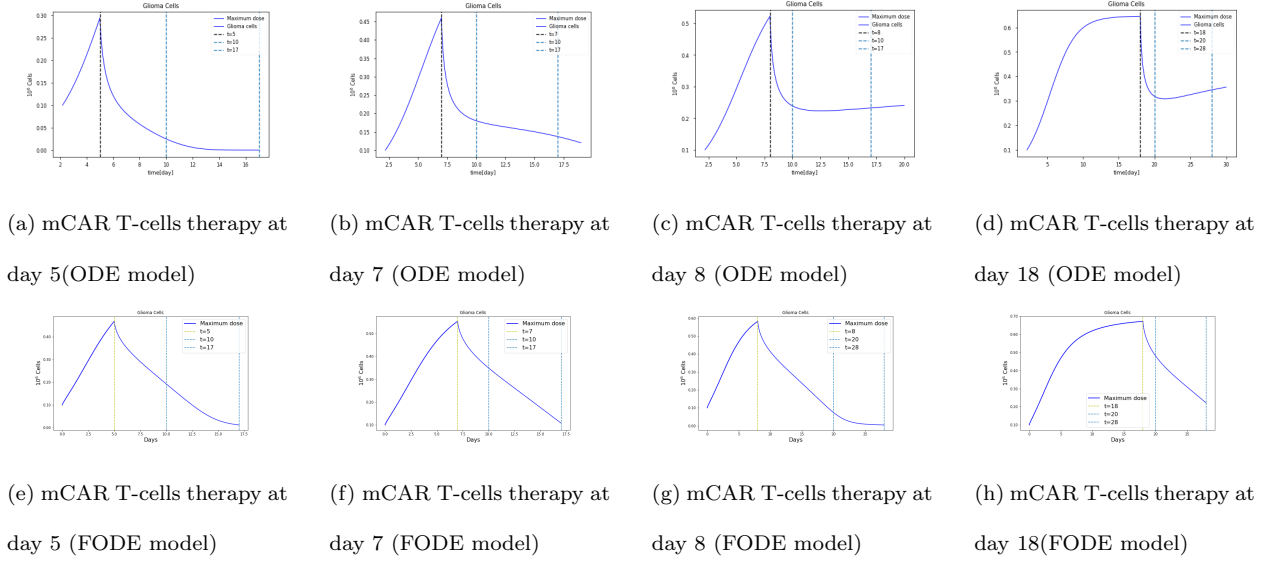


Figure 36: The impact of inoculation of mCAR T-cells on tumor progression in syngeneic glioma models using ODE and FODE models. (a),(b) KR70-C tumor progression after mCAR T-cell therapy at day 5 and day 7 of tumor inoculation using ODE model. (c),(d) KR70-B tumor progression after mCAR T-cell therapy at day 8 and day 18 of tumor inoculation using ODE model. (e),(f) KR70-C tumor progression after mCAR T-cell therapy at day 5 and day 7 of tumor inoculation using FODE model. (g),(h) KR70-B tumor progression after mCAR T-cell therapy at day 8 and day 18 of tumor inoculation using FODE model. When tumor burden is small, mCAR T-cell therapy is able to eliminate the tumor in both ODE and FODE models (a, b, e, f). However, when tumor burden is large, mCAR T-cell clear the tumor burden only in FODE model (g, h).

### 5.2.7 The number of injected CAR T-cells does affect treatment outcome

We next studied the dynamics of Equation (55) under different numbers of injected CAR T-cells. The model shows that the treatment is T-cells dependent which is in line with the findings in [22]. T-cells dependent is displayed in Figures 37. The change of the injected CAR T-cells load resulted in treatment results per mouse. A reduction in the time to peak for maximum dosage compare with low dosage. The higher the dosage of CAR T-cells lower the time peak.

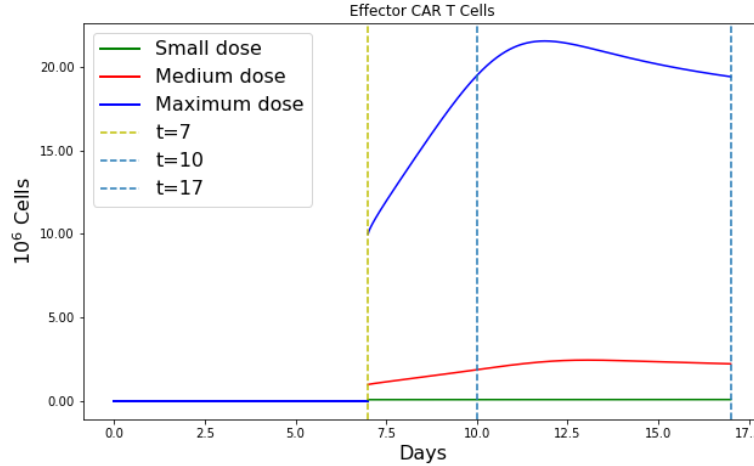


Figure 37: The immunotherapy with mCAR T on CD70+U87 glioma is performed on day 7. Soon after there is a decay of  $C_T$ , which is partially converted into  $C_M$ . There is an expansion of CAR T-cells, which can reduce growth and eliminate the tumor. (Data extracted from [22]).

We see the persistence of CAR T-cells for a long time. It has been described that when the number of CAR T-cells injected is small, the therapy can fail [22]. However, the injection of low CAR T-cells numbers is typically done when these cells do not expand well in-vitro, which could be the result of a low stimulation capability. We simulated the effect of injected CAR T-cells and the dynamics of treatment was substantially affected, see Figure 37. A

reduction in dosage of the CAR T-cells led to slower growth of this population, resulting in tumor growth reaching unacceptable levels without any pre-clinical response.

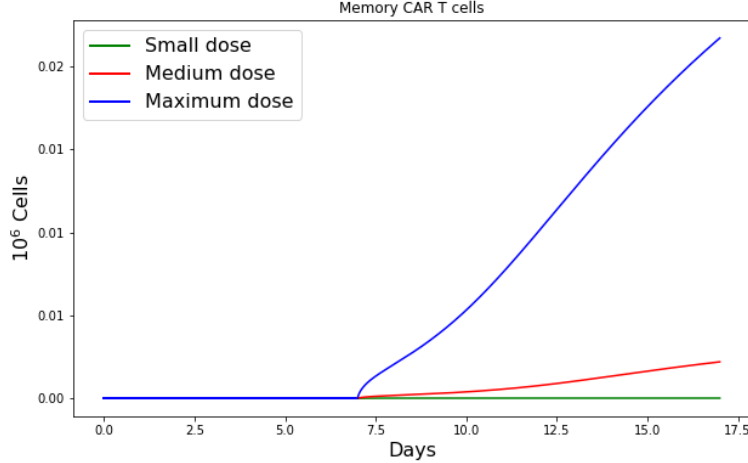


Figure 38: Dynamics Memory CAR T-cells under different dosages of CAR T-cells. The immunotherapy with hCAR T on CD70+U87 glioma. The tumor is rapidly eliminated after a medium  $10^6$  hCAR T-cells or a maximum  $10^7$  hCAR T-cells dose CAR T-cells.

### 5.2.8 Maximum expansion of Memory T-cells and CAR T-cells in vivo

We use system (55) to compute numerically the time  $t_{\max}$  at which CAR T-cells peak. At the time  $t_{\max}$ , occurs between 7 to 21 days (which contains a typical range in clinical studies) after injection of the CAR T-cells, the first maximum in their number, denoted by  $C_{T_{\max}} = C_T(t_{\max})$ , is achieved during the expansion phase. The time  $t_{\max}^l$  for the lower dosage injected CAR T-cells is larger than the time  $t_{\max}^m$ . The value of  $t_{\max}$  can be calculated from system (55) numerically.

Thus, the maximum number of CAR T-cells that can be achieved during the first expansion phase will be related to the initial tumor burden  $G_0$  and injected CAR T-cells  $C_{T_0}$ . Note

that the contribution of  $C_{T_0}$  is very significant. Thus, evidencing that the initial number of injected CAR T-cells does affect the peak.

It is easy to obtain numerical values to compute the tumor and memory T-cell loads in mice at time  $t_{\max}$ .

For managing toxicity, the maximum dose  $10^7$  CAR T-cells was most dose can be injected per mouse [22]. Figure 38 shows the linear dependence of the maximum number of CAR T-cells obtained from simulations of Equation (55). The above result points out to a proportionality dependence between the total tumor load and the treatment outcome. In fact, a strong correlation between disease burden at the time of CAR-T cell infusion and treatment outcome.

### **5.3 The effect of memory on the hCAR T-cell therapy against the glioma cells**

The fractional derivatives play a significant role in describing the effects of memory in dynamical systems. Also, The fractional derivative order  $\theta$  contributes to time delay in ordinary differential models [38], [33]. When the  $\theta$  value decreasing from 1, the memory effect of the system increases, it takes more time to reduce the number of tumor cells. So, the classical derivative solution gives a shorter period of disease We see from Fig. 39 that tumor cells reduce to close to zero more than 100 days from tumor inoculation for  $\theta = 0.70$ . However, for  $\theta = 1$ , the number of tumor cells reduced to close to zero for 20 days from tumor inoculation. When the  $\theta$  value decreasing, it takes more time to reduce the number of glioma cells. So, the classical derivative solution gives a shorter period of disease. When the derivative order

$\theta$  is reduced from 1, the memory effect of the system increases. Therefore, the results in Figures 39, 40, 41 and 42, we see that, impact of the derivative order  $\theta$  ( $0.7 \leq \theta \leq 1$ ) on the glioma cells, CAR T-cells and memory T-cells populations.

**5.3.1 The effect of memory on the tumor cells for different values of  $\theta$**

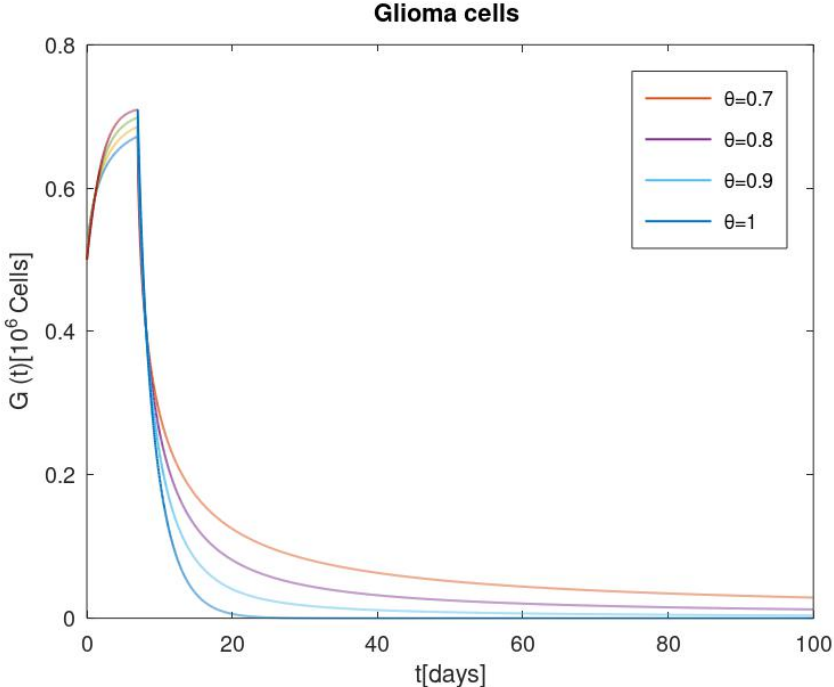


Figure 39: The dynamical behavior of tumor cells for varying values of the fractional-order parameter  $\theta$  for maximum dose of hCAR T-cell therapy over time. The total number of tumor cells are smaller in the case of  $\theta = 1.0$  than in the case of  $\theta = 0.7$ . When the derivative order  $\theta$  is reduced from 1, the memory effect of the system increases which leads time delay in the system.

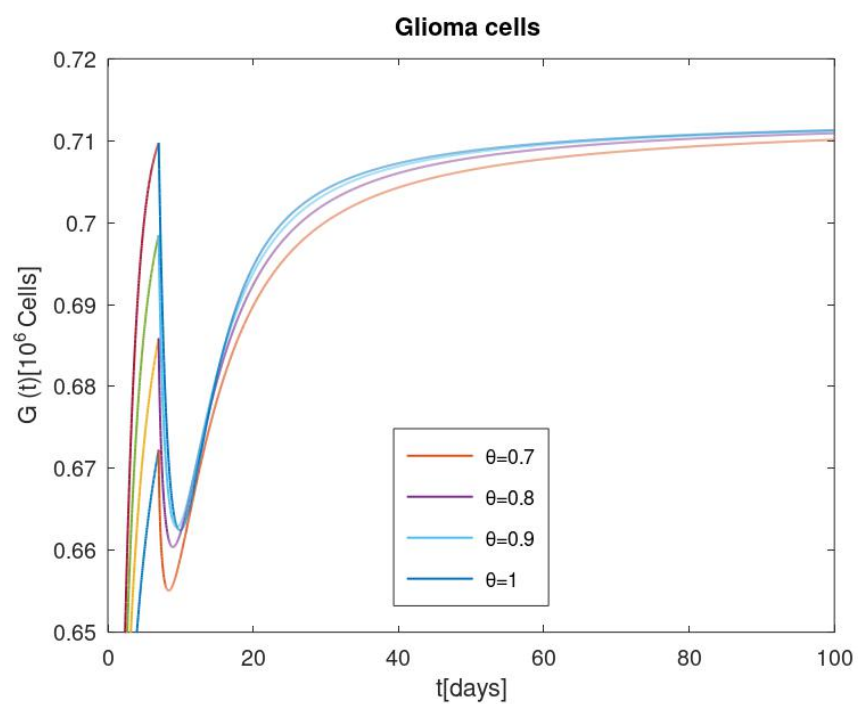


Figure 40: The dynamical behavior of tumor cells for varying values of the fractional-order parameter  $\theta$  for smaller dose of hCAR T-cell therapy over time. The total number of tumor cells are larger in the case of  $\theta = 1.0$  than in the case of  $\theta = 0.7$ . When the derivative order  $\theta$  is reduced from 1, the memory effect of the system increases, and the tumor cells decrease.

### 5.3.2 The effect of memory on the hCAR T-cells for different values of $\theta$

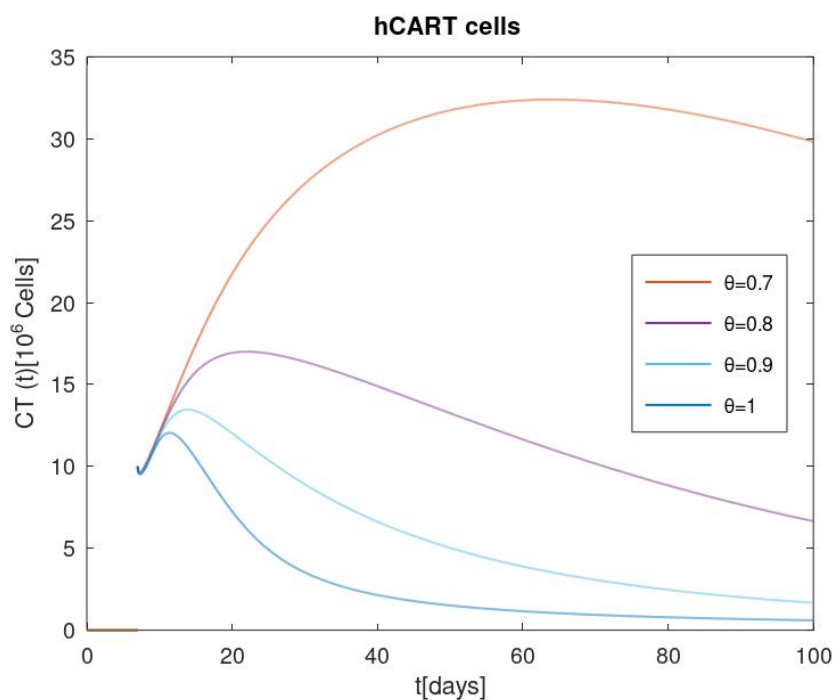


Figure 41: The dynamical behavior of hCAR T-cells for varying values of the fractional-order parameter  $\theta$  for maximum dose of hCAR T-cell therapy over time. When the derivative order  $\theta$  is reduced from 1, the memory effect of the system increases. Therefore, number of hCAR T-cells increases and hCAR T-cells persist for a long time in the system for  $\theta = .7$  than in the case of  $\theta = 1.0$  (integer order).

### 5.3.3 The effect of memory on the memory T-cells for different values of $\theta$

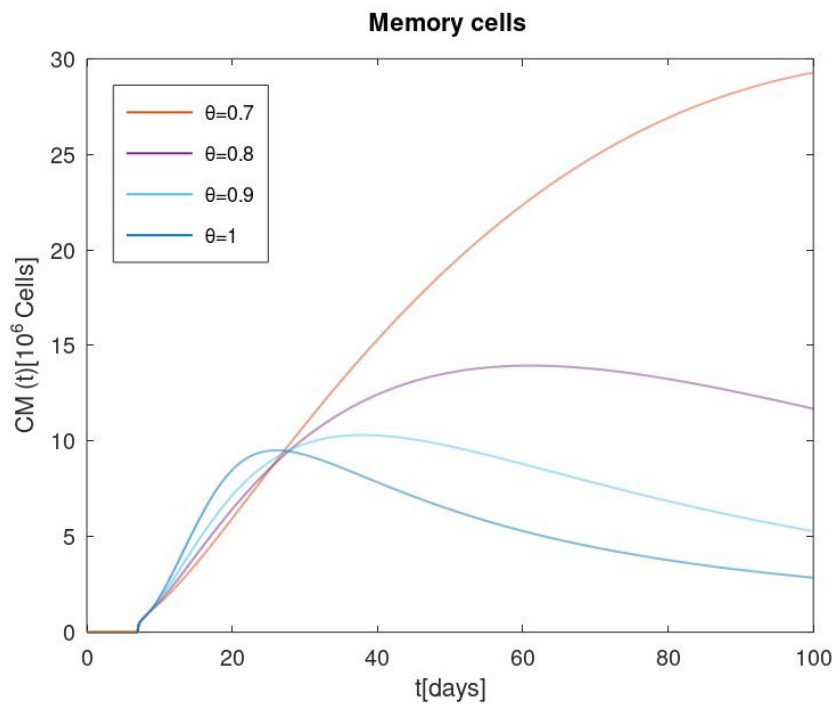


Figure 42: The dynamical behavior of memory T-cells for varying values of the fractional-order parameter  $\theta$  for maximum dose of hCAR T-cell therapy over time. When the derivative order  $\theta$  is reduced from 1, the memory effect of the system increases. Therefore, higher number of memory T-cells can be seen in the case of  $\theta = .7$  than in the case of  $\theta = 1.0$  (integer order).

## CHAPTER 6

### DISCUSSION

In 2020, Sahoo *et al* [41] modeled the dynamics between cancer cells and CAR T-cells as a predator prey system with the CARRGO mathematical model: Chimeric Antigen Receptor T-cells treatment Response in Glioma. Their model was two compartment model.

Our proposed six-compartment ODE and FODE models which focus on interaction between glioma cells, CAR T-cells, memory T-cells, macrophages, immune stimulating factor ( $IFN_\gamma$ ) and immune inhibiting factor ( $TGF_\beta$ ) were used to investigate the tumor response against CAR T-cell therapy in mouse models. In particular, human and mouse CAR T therapy which targets CD70 antigen in U87 and KR70 tumors were considered in this work. We used Beddington–DeAngelis functional response term for the tumor lysis by CAR T in our model to incorporate search time assuming CAR T-cells need time to identify tumor cells before destroying them. Before model simulations were performed, tumor growth rate ( $r$ ) and carrying capacity of the tumor ( $K_G$ ) were estimated assuming tumor grows logistically in the absence of the immune system using tumor data. In addition to the parameters of the Beddington DeAngelis functional response of CAR T-cells killing of glioma cells ( $d, s, l$  and  $w$ ) were estimated using previously published CAR T-cells data. We obtained some model parameter values from the published literature and estimated the remaining model parameters through the simulations of the six-compartment model.

We analyzed our models which consists of system of ordinary equations and fractional order differential equations for the steady states and determined the equilibrium points of the system and conditions for the stability of the equilibrium points. We consider a set of

parameter values, and found two equilibrium points for the models. An unstable tumor free equilibrium point where tumor cells do not disappear over the time and stable equilibrium point where tumor disappear over the time. We further found that the model exhibits bistability where a dosage threshold exists. A CAR T-cells dosage above the threshold can reduce to cancer free while below the threshold grows to a lethal size. Our simulated results show that small dosages of CD70 CAR T-cells is below the threshold, hence it is not able to eliminate the tumor burden. However, medium and large CAR T-cells dosages are above the threshold, hence inhibit the tumor burden completely.

Sobol's sensitivity analysis were performed on our six-compartment models considering glioma dynamics against human and mouse specific CAR T-cells to identify the key parameters that drive the model output. The Sobol's sensitivity analysis results of ODE model indicated that  $b_1$ ,  $\mu_T$ ,  $\mu_2$ ,  $\alpha_M$  and  $e_1$  are the parameters that contribute most significantly to the model output whereas the Sobol's sensitivity analysis results of FODE model indicated that most sensitive parameter is  $\alpha_M$  with the high scaled Sobol's index followed by  $b_1$  and  $\mu_2$ .

We simulated the models with three different CAR T-cells dosages against glioma lines considering two scenarios, one with three different human CD70 CAR T dosages against U87 glioma lines and another with the three different murine-derived CD70 CAR T dosages against KR70 glioma lines using data presented based on a published article from literature [22].

We have to point out that our study is limited. The investigation of CAR T-cell therapy of glioma mechanisms is still underway, and we still do not have a thorough understanding of this novel treatment. A better understanding of these mechanisms can help us better improve

the model in the future. There are many other mechanisms that we have overlooked in our model. Our estimation of parameters is based on various publications and many of them are in vitro studies. Moreover, these parameter values only reflect an average view though they may vary significantly from individual to individual. For example, the total number of cells, the percentage of CAR T-cells, and the production and clearance rates of immunostimulatory factor, immunosuppressive factor and tumor may be very different for different individuals.

In our FODE model, we chose Caputo fractional derivative because the immune system and also the cancer cells have memory features. This model is specialized in macrophages cells,  $I_\gamma$  and  $T_\beta$  because they are important parts of the immune system. Moreover, the model examines how CAR T-cells fight with tumor cells. The numerical solution of the model was found with the help of the Adam-Bashforth-Moulton algorithm for fractional-order model [37]. Different scenarios of the solution were displayed using graphs to visualize them. The effectiveness of the cells of immune system are increasing in contrast, the effectiveness of tumor cells are decreasing for different values of  $\theta$ . It is seen that the small change in  $\theta$  has great results and the approximate solution depend on the fractional order  $\theta$ . It has two reasons, either of them is the Caputo fractional derivative is appropriate real-life problem that is, it gives good results in such problems, the other is Caputo fractional derivative is non-local derivative.

In this study, we have developed ordinary differential equations (ODE) and fractional ordinary differential equations (FODE) models to study CAR T-cells response to tumor growth which is based on our understanding of the interaction between the immune system and tumor growth. We conclude that, the FODE model fits the data better and outperforms

the ODE model for animal data. Although we obtained better results using FODE approach, the numerical algorithms for solving FODEs are computationally expensive.

In future work, we will develop a mixture model which will consists of both system of ordinary differential equations (ODE) and fractional ordinary differential equations (FODE) to explore the CAR T-cells response to tumor growth. FODEs in the mixture model will model cells (CAR T-cells, memory T-cells and macrophages) which have memory structures and ODEs will model the stimulating and inhibiting factors ( $I_\gamma$  and  $T_\beta$  which have no memory structures).

## BIBLIOGRAPHY

## References

- [1] LG áDe Pillis. W. águ and ae áradunskaya. *J. Theor. Biol*, 2006.
- [2] Stephen J Bagley, Arati S Desai, Gerald P Linette, Carl H June, and Donald M O'Rourke. Car t-cell therapy for glioblastoma: recent clinical advances and future challenges. *Neuro-oncology*, 20(11):1429–1438, 2018.
- [3] Sandip Banerjee, Subhas Khajanchi, and Swapna Chaudhuri. A mathematical model to elucidate brain tumor abrogation by immunotherapy with t11 target structure. *PLoS One*, 10(5):e0123611, 2015.
- [4] John R Beddington. Mutual interference between parasites or predators and its effect on searching efficiency. *The Journal of Animal Ecology*, pages 331–340, 1975.
- [5] Christine E Brown, Darya Alizadeh, Renate Starr, Lihong Weng, Jamie R Wagner, Araceli Naranjo, Julie R Ostberg, M Suzette Blanchard, Julie Kilpatrick, Jennifer Simpson, et al. Regression of glioblastoma after chimeric antigen receptor t-cell therapy. *New England Journal of Medicine*, 375(26):2561–2569, 2016.
- [6] Michele Caputo. Linear models of dissipation whose  $q$  is almost frequency independent—ii. *Geophysical Journal International*, 13(5):529–539, 1967.

- [7] Karen Chan, Andrea Saltelli, and Stefano Tarantola. Sensitivity analysis of model output: variance-based methods make the difference. In *Proceedings of the 29th conference on Winter simulation*, pages 261–268, 1997.
- [8] Fabien Crauste, Julien Mafille, Lilia Boucinha, Sophia Djebali, Olivier Gandrillon, Jacqueline Marvel, and Christophe Arpin. Identification of nascent memory cd8 t cells and modeling of their ontogeny. *Cell systems*, 4(3):306–317, 2017.
- [9] Don L De Angelis. Stability and connectance in food web models. *Ecology*, 56(1):238–243, 1975.
- [10] Lisette G de Pillis and Ami Radunskaya. A mathematical model of immune response to tumor invasion. In *Computational fluid and solid mechanics 2003*, pages 1661–1668. Elsevier, 2003.
- [11] Lisette G de Pillis, Ami E Radunskaya, and Charles L Wiseman. A validated mathematical model of cell-mediated immune response to tumor growth. *Cancer research*, 65(17):7950–7958, 2005.
- [12] KE De Visser and WM Kast. Effects of  $\text{tgf-}\beta$  on the immune system: implications for cancer immunotherapy. *Leukemia*, 13(8):1188–1199, 1999.
- [13] Andreas Diefenbach, Eric R Jensen, Amanda M Jamieson, and David H Raulet. Rael and h60 ligands of the nkg2d receptor stimulate tumour immunity. *Nature*, 413(6852):165–171, 2001.

- [14] Kai Diethelm, Neville J Ford, and Alan D Freed. A predictor-corrector approach for the numerical solution of fractional differential equations. *Nonlinear Dynamics*, 29(1):3–22, 2002.
- [15] Kai Diethelm, Neville J Ford, and Alan D Freed. Detailed error analysis for a fractional adams method. *Numerical algorithms*, 36(1):31–52, 2004.
- [16] Amy R Dix, William H Brooks, Thomas L Roszman, and Lorri A Morford. Immune defects observed in patients with primary malignant brain tumors. *Journal of neuroimmunology*, 100(1-2):216–232, 1999.
- [17] Britta Engelhardt. Molecular mechanisms involved in t cell migration across the blood–brain barrier. *Journal of neural transmission*, 113(4):477–485, 2006.
- [18] Roberto Garrappa. Numerical solution of fractional differential equations: A survey and a software tutorial. *Mathematics*, 6(2):16, 2018.
- [19] Haitao Ge, Luyan Mu, Linchun Jin, Changlin Yang, Yifan Chang, Yu Long, Gabriel DeLeon, Loic Deleyrolle, Duane A Mitchell, Paul S Kubilis, et al. Tumor associated cd70 expression is involved in promoting tumor migration and macrophage infiltration in gbm. *International journal of cancer*, 141(7):1434–1444, 2017.
- [20] Toshimitsu Homma and Andrea Saltelli. Use of sobol’s quasirandom sequence generator for integration of modified uncertainty importance measure. *Journal of Nuclear Science and Technology*, 32(11):1164–1173, 1995.

- [21] AY Huang, Paul Golumbek, Mojgan Ahmadzadeh, Elizabeth Jaffee, Drew Pardoll, and Hyam Levitsky. Role of bone marrow-derived cells in presenting mhc class i-restricted tumor antigens. *Science*, 264(5161):961–965, 1994.
- [22] Linchun Jin, Haitao Ge, Yu Long, Changlin Yang, Yifan Chang, Luyan Mu, Elias J Sayour, Gabriel De Leon, Qiong J Wang, James C Yang, et al. Cd70, a novel target of car t-cell therapy for gliomas. *Neuro-oncology*, 20(1):55–65, 2018.
- [23] Linchun Jin, Haipeng Tao, Aida Karachi, Yu Long, Alicia Y Hou, Meng Na, Kyle A Dyson, Adam J Grippin, Loic P Deleyrolle, Wang Zhang, et al. Cxcr1-or cxcr2-modified car t cells co-opt il-8 for maximal antitumor efficacy in solid tumors. *Nature communications*, 10(1):1–13, 2019.
- [24] Erich Kamke. Zur theorie der systeme gewöhnlicher differentialgleichungen. ii. *Acta Mathematica*, 58(1):57–85, 1932.
- [25] Subhas Khajanchi and Sandip Banerjee. Quantifying the role of immunotherapeutic drug t11 target structure in progression of malignant gliomas: Mathematical modeling and dynamical perspective. *Mathematical Biosciences*, 289:69–77, 2017.
- [26] Denise Kirschner and John Carl Panetta. Modeling immunotherapy of the tumor-immune interaction. *Journal of mathematical biology*, 37(3):235–252, 1998.
- [27] Vladimir A Kuznetsov, Iliya A Makalkin, Mark A Taylor, and Alan S Perelson. Non-linear dynamics of immunogenic tumors: parameter estimation and global bifurcation analysis. *Bulletin of mathematical biology*, 56(2):295–321, 1994.

- [28] Andreas Mayer, Yaojun Zhang, Alan S Perelson, and Ned S Wingreen. Regulation of t cell expansion by antigen presentation dynamics. *Proceedings of the National Academy of Sciences*, 116(13):5914–5919, 2019.
- [29] Hongsheng Miao, Bryan D Choi, Carter M Suryadevara, Luis Sanchez-Perez, Shicheng Yang, Gabriel De Leon, Elias J Sayour, Roger McLendon, James E Herndon II, Patrick Healy, et al. Egfrviii-specific chimeric antigen receptor t cells migrate to and kill tumor deposits infiltrating the brain parenchyma in an invasive xenograft model of glioblastoma. *PloS one*, 9(4):e94281, 2014.
- [30] Connor Lawrence Mitchell. *Validation and Analysis of Numerical Methods for Solving Fractional-Order Differential Equations*. PhD thesis, 2018.
- [31] Joydeep Mukherjee, Sukla Dutta, Susobhan Sarkar, Zarina Begum, Anirban Ghosh, Samares Chaudhuri, and Swapna Chaudhuri. Preclinical changes in immunoreactivity and cellular architecture during the progressive development of intracranial neoplasms and an immunotherapeutic schedule with a novel biological response modifier, the t11ts/s-lfa3. *Asian Pacific Journal of Cancer Prevention*, 3:325–337, 2002.
- [32] Soranobu Ninomiya, Neeharika Narala, Leslie Huye, Shigeki Yagyu, Barbara Savoldo, Gianpietro Dotti, Helen E Heslop, Malcolm K Brenner, Cliona M Rooney, and Carlos A Ramos. Tumor indoleamine 2, 3-dioxygenase (ido) inhibits cd19-car t cells and is downregulated by lymphodepleting drugs. *Blood*, 125(25):3905–3916, 2015.
- [33] Ilhan Öztürk and Fatma Özköse. Stability analysis of fractional order mathematical model of tumor-immune system interaction. *Chaos, Solitons & Fractals*, 133:109614,

2020.

- [34] Florence Paillard. Commentary: Immunosuppression mediated by tumor cells: A challenge for immunotherapeutic approaches. *Human gene therapy*, 11(5):657–658, 2000.
- [35] Nathan D Pennock, Jason T White, Eric W Cross, Elizabeth E Cheney, Beth A Tamburini, and Ross M Kedl. T cell responses: naive to memory and everything in between. *Advances in physiology education*, 37(4):273–283, 2013.
- [36] Phillip K Peterson, Chun C Chao, Shuxian Hu, Kim Thielen, and Edward G Shaskan. Glioblastoma, transforming growth factor- $\beta$ , and candida meningitis: a potential link. *The American journal of medicine*, 92(3):262–264, 1992.
- [37] Igor Podlubny. *Fractional differential equations: an introduction to fractional derivatives, fractional differential equations, to methods of their solution and some of their applications*. Elsevier, 1998.
- [38] Fathalla A Rihan. Numerical modeling of fractional-order biological systems. In *Abstract and Applied Analysis*, volume 2013. Hindawi, 2013.
- [39] Brendon J Rodrigues, Luciana Rodrigues Carvalho Barros, and Regina Celia Almeida. Three-compartment model of car t-cell immunotherapy. *bioRxiv*, page 779793, 2020.
- [40] Marco Ruella, Michael Klichinsky, Saad S Kenderian, Olga Shestova, Amy Ziober, Daniel O Kraft, Michael Feldman, Mariusz A Wasik, Carl H June, and Saar Gill. Overcoming the immunosuppressive tumor microenvironment of hodgkin lymphoma using chimeric antigen receptor t cells. *Cancer discovery*, 7(10):1154–1167, 2017.

- [41] Prativa Sahoo, Xin Yang, Daniel Abler, Davide Maestrini, Vikram Adhikarla, David Frankhouser, Heyrim Cho, Vanessa Machuca, Dongrui Wang, Michael Barish, et al. Mathematical deconvolution of car t-cell proliferation and exhaustion from real-time killing assay data. *Journal of the Royal Society Interface*, 17(162):20190734, 2020.
- [42] Ilya M Sobol. Global sensitivity indices for nonlinear mathematical models and their monte carlo estimates. *Mathematics and computers in simulation*, 55(1-3):271–280, 2001.
- [43] Il'ya Meerovich Sobol'. On sensitivity estimation for nonlinear mathematical models. *Matematicheskoe modelirovanie*, 2(1):112–118, 1990.
- [44] Dhruv Sud, Carolyn Bigbee, JoAnne L Flynn, and Denise E Kirschner. Contribution of cd8+ t cells to control of mycobacterium tuberculosis infection. *The Journal of Immunology*, 176(7):4296–4314, 2006.
- [45] Corinne Tanchot, François A Lemonnier, Beatrice Pérarnau, Antonio A Freitas, and Benedita Rocha. Differential requirements for survival and proliferation of cd8 naive or memory t cells. *Science*, 276(5321):2057–2062, 1997.
- [46] Daniela S Thommen and Ton N Schumacher. T cell dysfunction in cancer. *Cancer cell*, 33(4):547–562, 2018.
- [47] Qiong J Wang, Zhiya Yu, Ken-ichi Hanada, Krishna Patel, David Kleiner, Nicholas P Restifo, and James C Yang. Preclinical evaluation of chimeric antigen receptors targeting cd70-expressing cancers. *Clinical Cancer Research*, 23(9):2267–2276, 2017.

- [48] Hsiu-Chuan Wei. Mathematical and numerical analysis of a mathematical model of mixed immunotherapy and chemotherapy of cancer. *Discrete & Continuous Dynamical Systems-B*, 21(4):1279, 2016.
- [49] Hsiu-Chuan Wei. A mathematical model of tumour growth with beddington–deangelis functional response: a case of cancer without disease. *Journal of Biological Dynamics*, 12(1):194–210, 2018.
- [50] Edmund Taylor Whittaker. Vito volterra, 1860-1940, 1941.
- [51] Santos B Yuste and Luis Acedo. An explicit finite difference method and a new von neumann-type stability analysis for fractional diffusion equations. *SIAM Journal on Numerical Analysis*, 42(5):1862–1874, 2005.
- [52] X-Y Zhang, Mirjam N Trame, Lawrence J Lesko, and Stephan Schmidt. Sobol sensitivity analysis: a tool to guide the development and evaluation of systems pharmacology models. *CPT: pharmacometrics & systems pharmacology*, 4(2):69–79, 2015.